Received: 3 December 2021 | Accepted: 13 January 2022

DOI: 10.1111/gcb.16121

Global Change Biology WILEY

RESEARCH ARTICLE

Satellite observations document trends consistent with a boreal forest biome shift

Logan T. Berner | Scott J. Goetz

School of Informatics, Computing, and Cyber Systems, Northern Arizona University, Flagstaff, Arizona, USA

Correspondence
Logan Berner, 1295 S. Knoles Drive, School of Informatics, Computing, and Cyber Systems, Northern Arizona University, Flagstaff, AZ 86011, USA.
Email: logan.berner@nau.edu

Funding information
National Aeronautics and Space Administration, Grant/Award Number: 80NSSC19M0112, NNX17AE13G and NNX17AE44G

Abstract

The boreal forest biome is a major component of Earth's biosphere and climate system that is projected to shift northward due to continued climate change over the coming century. Indicators of a biome shift will likely first be evident along the climatic margins of the boreal forest and include changes in vegetation productivity, mortality, and recruitment, as well as overall vegetation greenness. However, the extent to which a biome shift is already underway remains unclear because of the local nature of most field studies, sparsity of systematic ground-based ecological monitoring, and reliance on coarse resolution satellite observations. Here, we evaluated early indicators of a boreal forest biome shift using four decades of moderate resolution (30 m) satellite observations and biogeoclimatic spatial datasets. Specifically, we quantified interannual trends in annual maximum vegetation greenness using an ensemble of vegetation indices derived from Landsat observations at 100,000 sample sites in areas without signs of recent disturbance. We found vegetation greenness increased (greened) at 38 [29, 42] % and 22 [15, 26] % of sample sites from 1985 to 2019 and 2000 to 2019, whereas vegetation greenness decreased (browned) at 13 [9, 15] % and 15 [13, 19] % of sample sites during these respective periods [95% Monte Carlo confidence intervals]. Greening was thus 3.0 [2.6, 3.5] and 1.5 [0.8, 2.0] times more common than browning and primarily occurred in cold sparsely treed areas with high soil nitrogen and moderate summer warming. Conversely, browning primarily occurred in the climatically warmest margins of both the boreal forest biome and major forest types (e.g., evergreen conifer forests), especially in densely treed areas where summers became warmer and drier. These macroecological trends reflect underlying shifts in vegetation productivity, mortality, and recruitment that are consistent with early stages of a boreal biome shift.

KEYWORDS
Arctic Boreal Vulnerability Experiment (ABoVE), browning, climate change, ecotone, forest productivity, greening, Landsat, tree mortality, tree recruitment, warming

1 | INTRODUCTION

Climate change could drive major shifts in the geographic extents of terrestrial biomes over the coming century (Gonzalez et al., 2010; Koven, 2013), especially the boreal forest biome that has warmed more rapidly than nearly any other terrestrial domain (Gonzalez et al., 2010; Scheffer et al., 2012). The boreal forest biome covers ~15.1 million km^2 (Olson et al., 2001), comprises ~23% of global forest area (Sexton et al., 2016), accounts for ~55% of global forest area with low human pressure (Venter et al., 2016), and stores greater than 32% of all forest carbon (Bradshaw & Warkentin, 2015; Pan et al., 2013). Hence, boreal forests are a major component of Earth's terrestrial biosphere and climate system (Bonan, 2008), yet vulnerable to a biome shift as the climate continues to change (Baltzer et al., 2021; Gonzalez et al., 2010; Koven, 2013; Scheffer et al., 2012).

Warming and shifting water availability could cause forest losses and gains along the warmest and coolest climatic margins of the boreal forest biome, respectively (Beck et al., 2011; Scheffer et al., 2012; Tchebakova et al., 2009). Along the warmest margins, increasing heat and drought stress could initially decrease vegetation productivity and increase tree mortality rates (Kharuk et al., 2020; Peng et al., 2011), eventually causing forest conversion to woodlands, shrublands, or grasslands especially if disturbed (Baltzer et al., 2021; Scheffer et al., 2012). Conversely, along the coolest margins, warming could increase vegetation productivity and tree recruitment, gradually causing forest expansion into Arctic and alpine tundra. Field and satellite observations provide some evidence that such changes are already underway (Beck et al., 2011; Dial et al., 2007; Esper & Schweingruber, 2004; Frost & Epstein, 2014; Mamet et al., 2019), with a recent synthesis finding altitudinal or latitudinal treeline advance during the 20th century at 79 of 151 (i.e., 52%) study locations in the boreal forest–tundra ecotone (Rees et al., 2020). Ecosystem models predict further changes along the climatic margins of the boreal forest biome with continued climatic changes over the coming century (Foster et al., 2019; Gonzalez et al., 2010; Tchebakova et al., 2009). Nevertheless, the extent to which a biome shift is already underway remains unclear across the enormous boreal forest because of the local nature of most field studies, sparsity of systematic ground-based ecological monitoring, and reliance on coarse resolution satellite data.

Earth-observing satellites make it possible to assess multidecadal changes in vegetation greenness across the boreal forest that could provide evidence of an emerging biome shift. Remotely sensed metrics of vegetation greenness (e.g., Normalized Difference Vegetation Index [NDVI]) are indicators of vegetation productivity and mortality (Boyd et al., 2021; Rogers et al., 2018; Sellers, 1987). Therefore, if a biome shift is occurring, we expect [1] declining vegetation productivity and increasing mortality to cause long-term decreases in vegetation greenness (browning) along the warmest margins and [2] increasing productivity and recruitment to cause long-term increases in vegetation greenness (greening) in the forest–tundra ecotone (Beck et al., 2011). Greening and browning trends consistent with these expectations have been detected in Alaska, where they were corroborated by long-term changes in tree growth (Beck et al., 2011). Pan-boreal greening and browning trends broadly consistent with these expectations have been detected over the past four decades using NDVI derived from spectral measurements made by the Advanced Very High Resolution Radiometers (AVHRR) (Beck & Goetz, 2011; Bunn & Goetz, 2006). However, boreal greening and browning trends are strongly influenced by forest disturbance (e.g., wildfire, harvest) and subsequent succession that fundamentally hinder efforts to detect a biome shift using coarse spatial resolution (generally ~8 km) AVHRR NDVI (Sulla-Menashe et al., 2017; Wang & Friedl, 2019). Furthermore, there is substantial uncertainty in AVHRR NDVI time series partly because of challenges with cross-calibrating measurements from sensors on 16 different satellites (Guay et al., 2014). Therefore, to detect an emerging biome shift, efforts are needed to assess pan-boreal changes in vegetation greenness using well-calibrated higher resolution satellite measurements (National Academies of Sciences, 2019).

The Landsat satellites and new metrics of vegetation greenness could provide further insight into the extent and potential drivers of an emerging boreal biome shift. The sensors on Landsat 5, 7, and 8 together provide 30-m resolution measurements of surface reflectance across most of Earth's land surface since the early 1980s (Wulder et al., 2019). This spatial resolution makes it more possible to account for impacts of disturbance and succession when evaluating vegetation greenness trends (Fiore et al., 2020; Sulla-Menashe et al., 2017; Wang & Friedl, 2019). Moreover, recent advances in cloud computing (Gorelick et al., 2017) and data processing techniques (Berner et al., 2020; Zhu et al., 2015) have facilitated large-scale analyses using the Landsat satellites (Berner et al., 2020; Hansen et al., 2013; Pastick et al., 2019) by helping to overcome issues with large amounts of data, low temporal resolution (~16 days), and lingering need for cross-sensor calibration (Berner et al., 2020; Ju & Masek, 2016). Also, compared with NDVI, there are newer vegetation indices (e.g., EVI2, NIRv, kNDVI) that may be better indictors of vegetation productivity (Badgley et al., 2017; Camps-Valls et al., 2021; Jiang et al., 2008). Despite these advances, pan-boreal changes in vegetation greenness potentially associated with early stages of a biome shift have yet to be assessed using the Landsat satellites.

Here, we evaluated changes in annual maximum vegetation greenness and their links with environmental drivers at recently undisturbed sample sites distributed across the boreal forest biome using nearly four decades of Landsat satellite imagery and environmental datasets (Figure 1). Specifically, we examined (i) the extent that vegetation greenness changed from 1985 to 2019 and 2000 to 2019; (ii) how changes varied with tree cover, land cover, and mean summer warmth; and (iii) the degree that greening and browning were associated with potential environmental drivers including climate, soils, and topography. We hypothesized there is an emerging boreal forest shift that includes browning in areas with high summer temperatures and dense tree cover, as well as greening in areas with low summer temperatures and sparse tree cover. Our analysis revealed changes in vegetation greenness during the last several

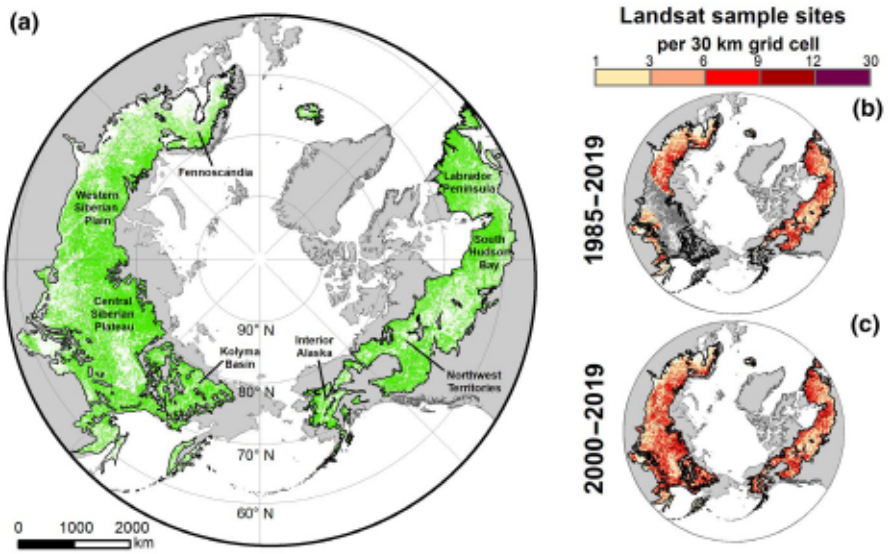

FIGURE 1 Spatial extent of boreal forest study domain and locations of Landsat sample sites. (a) Boreal forest stretches across northern Eurasia and North America to form one of Earth's largest terrestrial biomes (15.1 million km^2). The boreal study domain (green) included natural vegetation with low human pressure and no detectable disturbance since the early 1980s (8.4 million km^2). Lands in the boreal forest that were masked from analysis are shown in white. (b,c) Locations of Landsat sample sites that were used for assessing changes in vegetation greenness from (b) 1985 to 2019 and (c) 2000 to 2019, shown here as the number of sample sites in a 30 x 30 km grid cell. Lands in the boreal forest without adequate data for time series analysis are shown in dark gray. The spatial extent of the boreal forest biome is from the World Wildlife Foundation's Terrestrial Ecoregions of the World dataset (Olson et al., 2001). Map Projection: North Pole Lambert Azimuthal Equal Area

TABLE 1 Geospatial datasets used to mask nonvegetated land cover, anthropogenic land cover, and recently disturbed areas from the analysis

Description	Period	Resolution (m)	Reference
Global Land Cover	2018	300	ESA (2017)
Global Human Footprint	2009	1000	Venter et al. (2016)
Global Forest Change	2001–2019	30	Hansen et al. (2013)
Global MODIS Burned Area	2000–2019	500	Giglio et al. (2018)
Alaskan Large Fires	1984–2019	---	Kasischke et al. (2002)
Canadian Landsat Disturbance	1984–2015	30	Guindon et al. (2017)
Russian Young Forests	1985–2012	500	Loboda and Chen (2016)

decades that are consistent with early stages of a boreal biome shift. An ongoing biome shift could have wide-ranging implications for biodiversity, hydrology, permafrost, climate feedbacks, and communities across the high northern latitudes.

2 | MATERIALS AND METHODS

2.1 | Identifying recently undisturbed areas in the boreal forest

Our objective was to evaluate changes in vegetation greenness over the past four decades across recently undisturbed areas with natural vegetation in the boreal forest biome. The boreal forest spans ~15.1 million km^2 (Olson et al., 2001) and includes a mosaic of forest and nonforest land cover classes in various states of recovery from prior disturbances (e.g., wildfires, harvest) (Sulla-Menashe et al., 2017; Wang et al., 2019). We defined the spatial extent of the boreal forest biome using the Terrestrial Ecoregions of the World dataset (Olson et al., 2001) gridded at 300-m resolution in a North Pole Lambert Azimuthal Equal Area projection. Drawing on regional and global geospatial datasets (Table 1), we then applied a series of masks to exclude grid cells with nonvegetated or anthropogenic land cover (ESA, 2017), as well as grid cells with evidence of human pressure (Venter et al., 2016) or disturbance since the early 1980s (Giglio et al., 2018; Guindon et al., 2017; Hansen et al., 2013; Kasischke et al., 2002; Loboda & Chen, 2016). We resampled several 30-m resolution disturbance datasets to the 300-m grid and excluded grid cells with any evidence of disturbance. The MODIS burned area (Giglio et al., 2018) and Russian Young Forest (Loboda & Chen, 2016) datasets were originally gridded at 500-m resolution. To account for potential unrecorded disturbance in adjacent grid cells, we grew each disturbed grid cell outward by one grid cell in every direction and then masked out these grid cells. After masking out

nonvegetated, anthropogenic, and potentially disturbed areas, our resulting study area (sampling frame) comprised 56% (8.43 million km^2) of the boreal forest biome (Figure 1a). We processed geospatial data with the *raster* (Hijmans, 2019) and *gdalUtilities* (O'Brien, 2019) packages in the statistical software R (version 4.0) (R Core Team, 2021), with subsequent data handling and visualization facilitated by the packages *data.table* (Dowle & Srinivasan, 2021), *dplyr* (Wickham et al., 2021), *tidyr* (Wickham, 2021), *ggplot2* (Wickham, 2016), and *ggpubr* (Kassambara, 2020).

2.2 | Generating time series of annual maximum vegetation greenness using the Landsat satellites

We developed time series of annual maximum vegetation greenness from 1985 to 2019 for 10^5 random sample sites using 30-m resolution measurements of land surface reflectance from Landsat 5, 7, and 8. We focused on annual maximum vegetation greenness because it correlates with vegetation productivity and mortality (Berner et al., 2020; Boyd et al., 2021; Erasmi et al., 2021) and can be reliably estimated with Landsat data (Berner et al., 2020), whereas metrics like annual integrated growing season vegetation greenness are not readily derived using these satellite data given their low temporal resolution. Landsat surface reflectance data were produced by the United States Geological Survey (USGS) as part of the Landsat Collection 2 (Tier 1 and Tier 2) dataset that included corrections for atmospheric and terrain effects based on the Landsat Ecosystem Disturbance Adaptive Processing System (Masek et al., 2006) and Landsat 8 Surface Reflectance Code (Vermote et al., 2016). We generated 10^5 random sample sites across the sampling frame. Each sample site had a 900-m^2 footprint, indicating the total area across all sample sites was 90 km^2 or ~0.001% of the sampling frame (Figure 1b,c). For each sample site, we then extracted all Landsat surface reflectance measurements acquired June through August (days of year 152–243) between 1985 and 2019, for a total of 41.6 million multispectral surface reflectance measurements across all sample sites. Landsat data were extracted from the archive on Google Earth Engine (Gorelick et al., 2017) using the *rgee* interface (Aybar et al., 2020) accessed through the *lsatTS* package in R (Berner et al., 2022).

After extracting Landsat data for each sample site, we then filtered out unusable measurements using pixel- and scene-level criteria following workflows developed as part of several studies (Berner et al., 2018, 2020). Specifically, we filtered out observations affected by clouds, cloud shadows, surface water, or snow using the Function of Mask (Fmask) algorithm (Zhu et al., 2015) and further masked residual water using a Landsat-based global surface water dataset (Pekel et al., 2016). We also excluded measurements with suspiciously low (<0.005) or high (>1) surface reflectance, as well as measurements from scenes with >80% cloud cover, >30-m geometric uncertainty, >60° solar zenith angle. Data cleaning was conducted using the *lsatTS* package in R (Berner et al., 2022). In total, there were 16.6 million clear-sky, multispectral surface reflectance measurements across all sample sites.

We developed time series of annual maximum vegetation greenness for each sample site using clear-sky surface reflectance measurements in a Monte Carlo uncertainty framework. Estimates of annual maximum vegetation greenness are influenced by multiple sources of uncertainty that include sensor radiometric calibration, the selected metric of vegetation greenness (e.g., NDVI, EVI2), systematic differences in vegetation greenness among sensors, and the timing and availability of measurements. We therefore propagated these sources of uncertainty through our analysis using Monte Carlo simulations ($n = 10^3$) and used recently developed techniques to cross-calibrate vegetation indices among sensors and estimate annual maximum vegetation greenness (Berner et al., 2020). The Monte Carlo simulations were performed using a high-performance computing cluster at Northern Arizona University with cross-sensor calibration and phenological modeling implemented using algorithms from the *lsatTS* package in R (Berner et al., 2022). The approaches for cross-sensor calibration and phenological modeling are briefly described below, with additional details provided in Berner et al. (2020).

For each simulation, we randomly selected 90% of surface reflectance measurements at every sample site and then randomly permuted red and near infrared reflectance measurements by up to ±7%, 5%, or 3% for Landsat 5, 7, and 8, respectively (Markham et al., 2014; Markham & Helder, 2012). We then derived one of four randomly selected vegetation indices that included NDVI (Rouse et al., 1974), EVI2 (Jiang et al., 2008), NIRv (Badgley et al., 2017), and kNDVI (Camps-Valls et al., 2021). To address systematic differences in vegetation indices among sensors that could introduce spurious greening trends (Figures S1–S4), we cross-calibrated each vegetation index using a machine learning approach that matches Landsat 5/8 to Landsat 7, which is used as a benchmark because it temporally overlaps multiple years with the other sensors. Briefly, this approach involves identifying years when Landsat 5/8 and Landsat 7 both imaged a sample site, and then for each sensor computing the median vegetation index across these years focusing on a randomly selected, well-sampled 15-day period during summer. A Random Forest machine learning model is then trained to predict the median vegetation index from Landsat 7 based on the median vegetation index from Landsat 5/8 and information on the timing of each 15-day period and the spatial location of each sample site. Cross-validation showed that for each vegetation index, these models effectively minimized biases among sensors (Figures S1–S4, Table S1).

We estimated annual maximum vegetation greenness at each sample site using phenological modeling that prevents spurious greening trends due to increasing available of Landsat scenes over time (Berner et al., 2020). For each sample site, this approach iteratively pooled observations over multiple years (n = 5, 7, or 9 years), fit cubic splines of varying stiffness (spar = 0.65–0.75) that described the seasonal land surface phenology during those years, and then estimated maximum vegetation greenness for each year by adjusting individual observations from that year based on the phenological timing of their acquisition. Previous evaluation showed that this approach yielded robust estimates

of annual maximum vegetation greenness even when few observations are available from a single growing season (Berner et al., 2020). Overall, this approach enabled us to develop time series of annual maximum vegetation greenness that could be used to rigorously evaluate recent greening and browning trends, and trend uncertainty, across the boreal forest biome.

2.3 | Analyzing vegetation greenness trends

We assessed temporal trends in annual maximum vegetation greenness from 1985 to 2019 and 2000 to 2019 using Landsat satellite measurements from sample sites located in recently undisturbed areas across the boreal forest biome. These periods enabled the assessment of changes over the available record of Landsat 5, 7, and 8, as well as over the first 20 years of the 21st century when there is improved spatial coverage of observations. For every Monte Carlo simulation ($n = 10^3$), we tested each vegetation greenness time series for the presence of a monotonic trend during both periods using rank-based Mann–Kendall trend tests and Theil–Sen slope estimators following the removal of temporal autocorrelation (Yue et al., 2002). These steps were implemented using the *zyp* package in R (Bronaugh & Werner, 2019). We then classified changes in vegetation greenness at each sample site during both periods as greening, no trend, or browning based on the sign and significance (= .10) of the trend assessment. This general approach for time series analysis is less sensitive to outliers than ordinary least squares regression and has been widely used in prior remote sensing assessments of vegetation greenness trends in high northern latitude ecosystems (Berner et al., 2013; Forkel et al., 2013; Guay et al., 2014).

To visualize spatial patterns of vegetation greenness trends, we stratified the sample sites by ecological land unit (ELU) and then summarized changes within each ELU. The Global ELU dataset identifies areas with similar ecophysiographic conditions (Sayre et al., 2014). We majority resampled the ELU dataset from 30-m resolution to our 300-m grid and then masked out nonvegetated, anthropogenic, and potentially disturbed areas as described above. There were 431 unique ELUs in our study domain. After stratifying sample sites by ELU, we then computed and mapped not only the percentage of sample sites that greened or browned but also the median percent change in vegetation indices among sample sites in each ELU. These were effective means of summarizing patterns of change across a large network of sample sites.

2.4 | Summarizing vegetation greenness trends by land cover and tree cover

To better understand biological conditions associated with recent greening and browning, we assessed how changes in vegetation greenness varied with land cover class and tree cover across recently undisturbed sample sites in the boreal forest biome. For these analyses, we focused on changes in vegetation greenness from 2000 to 2019 rather than 1985 to 2019 because there is improved spatial coverage of Landsat data in the 2000s (Wulder et al., 2016) and greenness trends during the more recent period are likely less affected by vegetation recovery following disturbances in the 1960s and 1970s (Fiore et al., 2020; Sulla-Menashe et al., 2017). We characterized land cover class using the European Space Agency's Climate Change Initiative Land Cover dataset that represented conditions in 2018 at 300-m spatial resolution (ESA, 2017). This dataset includes 37 land cover classes that we consolidated to 10 simplified classes including deciduous broadleaf forest (DBF), deciduous needleleaf forest (DNF), evergreen needleleaf forest (ENF), mixed forest (MF), mosaic vegetation, shrublands, grasslands, wetlands, sparse vegetation, and other (e.g., urban areas, baren areas, water). The primary types of trees in DBF include aspen and birch (e.g., *Populus tremula*, *P. tremuloides*, *Betula* spp.), while DNF is composed of larch (e.g., *Larix cajanderi*, *L. gmelinii*, *L. sibirica*), and ENF is mostly composed of spruce (e.g., *Picea glauca*, *P. mariana*, *P. obovata*) and pine (e.g., *Pinus banksiana*, *P. sylvestris*, *P. sibirica*). For every Monte Carlo simulation ($n = 10^3$), we computed the absolute and relative occurrences of sample sites that greened, had no trend, or browned in each land cover class. We then derived best estimates (medians) and 95% confidence intervals (2.5th and 97.5th percentiles) of the absolute and relative occurrence of each trend class in every land cover class by summarizing across Monte Carlo simulations. Overall, this allowed us to characterize not only the absolute and relative extent of recent greening and browning in each land cover class but also the uncertainty associated with these estimates.

We examined how recent change in vegetation greenness varied with tree cover. Here, we used tree cover based on the MODIS Vegetation Continuous Fields dataset that represented conditions averaged from 2017 to 2019 at 250-m spatial resolution (DiMiceli et al., 2021). First, we estimated average tree cover across sample sites that greened, had no trend, or browned while also determining the 95% confidence intervals around these estimates using the Monte Carlo simulations. Next, we examined how the prevalence (i.e., relative occurrence) of greening and browning varied along spatial gradients of increasing tree cover with tree cover binned at 1% increments. We again computed best estimates (medians) and 95% confidence intervals using the Monte Carlo simulations. We also assessed the association between tree cover and the prevalence of greening and browning using Pearson's correlations computed using each Monte Carlo simulation. This analysis provided multiple perspectives on how recent greening and browning were related to current tree cover across the domain.

2.5 | Potential topoclimatic drivers of changes in vegetation greenness

We explored possible drivers of changes in vegetation greenness among sample sites using Random Forest models (Breiman,

2001) to predict the vegetation greenness trend class (i.e., greening or browning) from 2000 to 2019 based on climate, soil, and topography. We used climatic predictors that included averages, changes, and maximum anomalies in the summer warmth index (SWI; °C), summer vapor pressure deficit (VPD; kPa), summer soil moisture (cm), and annual water deficit (cm) from 2000 to 2019 derived from monthly TerraClimate data gridded at 4-km resolution (Abatzoglou et al., 2018). The SWI is a metric of growing season heat load that is computed as the annual sum of mean monthly air temperatures across all months exceeding 0°C (Walker et al., 2003), which can extend from roughly April through October in the southern boreal forest and June through September in the northern boreal forest. The SWI is widely used in Arctic and boreal ecological research (e.g., Berner et al., 2020; Keenan & Riley, 2018; Raynolds et al., 2008) and is similar to growing degree days but computed using monthly rather than daily temperature data. For each climatic predictor, the direction and magnitude of change from 2000 to 2019 were determined for every grid cell using Theil–Sen slope estimators. The magnitude of extreme heat and drought stress was also derived using the 20-year maximum (SWI, water deficit, VPD) or minimum (soil moisture) standardized anomaly (i.e., z-score) for each grid cell. Additional predictors included mean annual surface soil temperature from 2000 to 2016 (Obu et al., 2018) and soil nitrogen content at standard depths (0–5 cm, 5–15 cm, 15–30 cm) (Hengl et al., 2017). Soil nitrogen at 15–30 cm was strongly correlated (r = .83–.93) with nitrogen at deeper depths (30–60 cm, 60–100 cm, and 100–200 cm), so the deeper depths were not included. Topographic predictors included elevation, slope, eastness, and southness from the Global Multi-resolution Terrain Elevation Data (GMTED2010) (Danielson & Gesch, 2011). Pairwise correlations between all predictors were $r \leq .70$. In total, we used 20 predictor variables in the Random Forest models. This general approach builds on our prior efforts to explore drivers of recent vegetation greening and browning across the Arctic tundra biome (Berner et al., 2020).

We focused on sample sites that either greened or browned and trained a unique Random Forest classification model for every Monte Carlo simulation ($n = 10^3$). More sample sites greened than browned, so we balanced the sample size between trend classes by randomly selecting the same number of sample sites that greened as that browned. We randomly selected sample sites for model training (75%) and evaluation (25%) and then tuned the Random Forest models by determining the number of variables to assess at each node to optimize classification accuracy. We selected the model with the highest out-of-bag classification accuracy and then cross-validated the model with data that was withheld for evaluation. Finally, we assessed variable importance using the mean decrease in accuracy metric and produced partial dependency plots that describe how the classification probability of each class changes over the range of each predictor while keeping other predictors at their mean value. This processes relied on tools from the R packages *randomForest* (Liaw & Wiener, 2002), *caret* (Kuhn, 2008), and *pdp* (Greenwell, 2017).

3 | RESULTS

3.1 | Vegetation greenness trends in recently undisturbed boreal forest

Our analysis of Landsat satellite observations revealed widespread changes in vegetation greenness during the past four decades across recently undisturbed natural vegetation in the boreal forest biome (Figure 2). Landsat observations were not available across much of eastern Eurasia and Alaska prior to the year 2000, and thus for these regions, we did not assess changes in vegetation from 1985 to 2019 but did from 2000 to 2019 (Figure 1b,c). Across sample sites, median vegetation greenness increased 5.2 [2.3, 7.7] % from 1985 to 2019 and 1.7 [−0.8, 3.6] % from 2000 to 2019, or 0.15 [0.06, 0.22] % yr^{-1} and 0.08 [−0.04, 0.18] % yr^{-1} during these two periods, respectively [95% Monte Carlo confidence intervals]. Similar changes in median vegetation greenness were evident from 2000 to 2019 whether we examined all sample sites or only sample sites used to assess changes from 1985 to 2019 (i.e., 0.08 [−0.04, 0.18] % yr^{-1} vs. 0.07 [−0.06, 0.14] % yr^{-1}).

Vegetation greenness increased (critical value [ ] = .10; greened) at 38 [29, 42] % and 22 [15, 26] % of sample sites from 1985 to 2019 and 2000 to 2019, respectively. Conversely, vegetation greenness decreased (= .10; browned) at 13 [9, 15] % and 15 [13, 19] % of sample sites during these respective periods. There were no systematic trends in vegetation greenness (= .10) at the remaining 48 [44, 61] % and 64 [61, 67] % of sites during these periods. Greening was thus 3.0 [2.6, 3.5] times more common than browning from 1985 to 2019 and 1.5 [0.8, 2.0] times more common from 2000 to 2019. Summaries for each vegetation index of the ensemble are provided in Table S2.

Regional hotspots of changes in vegetation greenness were evident. Greening hotspots including parts of the West Siberian Plain, northern Central Siberian Plateau, and Kolyma Basin in northern Eurasia, as well as the Labrador Peninsula and Northwest Territories in North America (Figure 2a,c,d,f). Browning hotspots included the eastern Central Siberian Plateau in Eurasia, as well as eastern interior Alaska and areas south of Great Slave Lake and Hudson Bay in North America (Figure 2b,c,e,f). On average, greening occurred in more northern latitudes (60.7 [59.0, 60.8] °N) than browning (58.0 [57.7, 58.3] °N) from 2000 to 2019.

3.2 | Vegetation greenness trends related to tree cover

Greening and browning from 2000 to 2019 generally occurred at sample sites with sparse and moderate tree cover, respectively (Figure 3a,b,c). Tree cover averaged 25 [22, 27] % at sample sites that greened and 40 [39, 41] % at sample sites that browned (Figure 3b). Moreover, the prevalence of greening and browning markedly changed along spatial gradients in tree cover

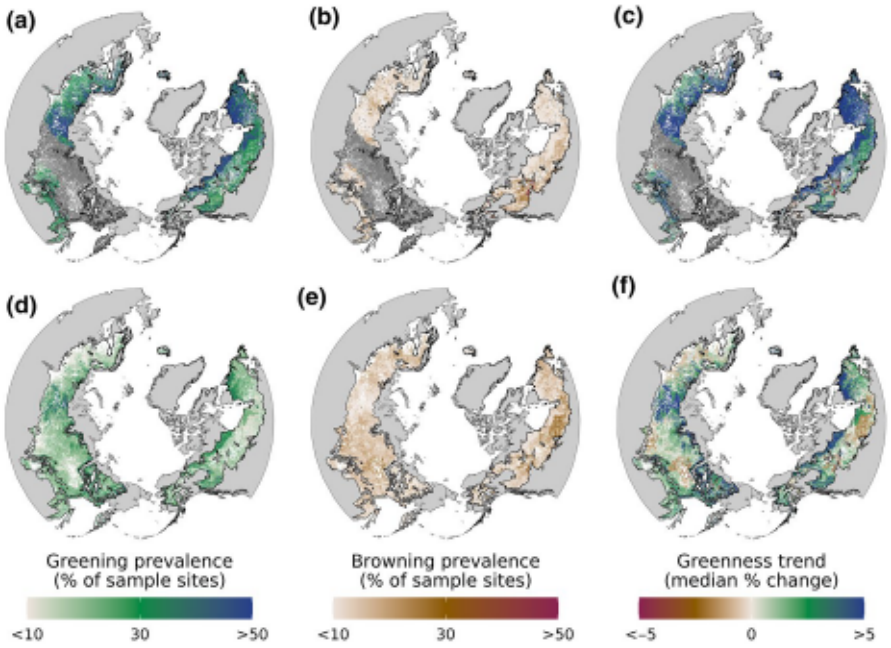

FIGURE 2 Changes in vegetation greenness during recent decades across the boreal forest biome. Changes in vegetation greenness were assessed from 1985 to 2019 (top row) and 2000 to 2019 (bottom row) at sample sites in recently undisturbed boreal forest using Mann–Kendall trend tests and Theil–Sen slopes. For visualization, the sample sites were grouped (i.e., stratified) and their trends summarized by ecological land unit (ELU), where each ELU is a distinct combination of bioclimate, landform, lithology, and land cover (Sayre et al., 2014). (a, d) Prevalence of greening within each ELU, specifically the percent of sample sites where vegetation greenness significantly (= .10) increased over each period. (b, e) Prevalence of browning within each ELU, specifically the percent of sample sites where vegetation greenness significantly (= .10) decreased over each period. (c, f) Overall magnitude of change in vegetation greenness within each ELU characterized by the median total percent change in vegetation greenness over each period. Panels (a, b, d, e) characterize how common significant changes in vegetation greenness were within each ELU, while panels (c, f) characterize the typical magnitude of change in vegetation greenness. There were 431 ELUs in the study domain

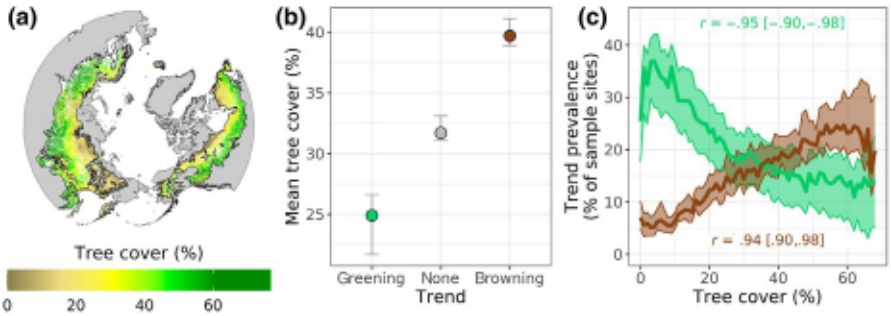

FIGURE 3 Vegetation greenness trends related to tree cover. (a) Tree cover across the boreal forest biome. (b) Mean tree cover across sample sites where vegetation greenness significantly (= .10) increased (greening), exhibited no trend, or decreased (browning) from 2000 to 2019. (c) Prevalence (i.e., relative frequency) of greening and browning along spatial gradients in tree cover binned at 1% increments. Correlation coefficients (r) between tree cover and the prevalence of greening and browning. Tree cover exceeded 68% at 1% of sample sites and these were excluded when correlations were computed given the small number of sample sites within each 1% tree cover bin. The panels depict best estimates (dots or lines) and 95% confidence intervals (whiskers or bands) derived from Monte Carlo simulations ($n = 10^3$). Tree cover data from the MODIS Vegetation Continuous Fields dataset (DiMiceli et al., 2021)

(Figure 3c). Specifically, with tree cover binned at 1% increments, an increase in tree cover was associated with decreased prevalence of greening ($r = -.95$ [−.90, −.98]) and increased prevalence of browning ($r = .94$ [.90, .98]; Figure 3c). For example, moving from sample sites with 5% tree cover to those with 65% tree cover, the prevalence of greening decreased from 35 [28, 42] % to 15 [5, 20] % while the prevalence of browning increased from 6 [5, 9] % to 20 [16, 33] %. Overall, there were pronounced differences in tree cover between areas that greened versus browned.

3.3 | Vegetation greenness trends related to land cover class

The study domain was primarily (65%) composed of two forest types that accounted for much of the greening and browning from 2000 to 2019 (Figure 4a,b). These included evergreen needleleaf forest (ENF) that comprised 36% of all sample sites and accounted for 29 [26, 32] % and 44 [41, 47] % of all greening and browning, respectively. Deciduous needleleaf forest (DNF) comprised 29% of all sample sites and accounted for 31 [28, 37] % and 28 [25, 30] % of all recent greening and browning, respectively. Mixed forests (MF) of needleleaf and broadleaf trees made up only 6% of all sample sites, but accounted for 10 [9, 11] % of all browning. The other six land cover classes each made up 1–9% of all sample sites and each accounted for less than 10% of all greening or browning (Figure 4b).

The prevalence (i.e., relative occurrence) of greening and browning from 2000 to 2019 widely varied among land cover classes across the biome (Figure 4c, Table S3). Greening was particularly prevalent in cold nonforest land cover classes including sparse vegetation, shrublands, and grasslands, where depending on land cover class, it occurred at 27 [19, 33] % to 38 [26, 44] % of sample sites and was 3.9 [2.1, 6.1] to 7.9 [3.0, 12.4] times more common than browning (Table S3). Greening was also more prevalent in deciduous needleleaf forests than any other forest class, with greening at 23 [19, 26] % of sample sites and about twice as common as browning. Browning was most prevalent in mixed-forest and deciduous broadleaf forest, where it occurred at 25 [22, 29] % and 21 [18, 27] % of sample sites, respectively. Greening was about half as common as browning in these two forest classes (Table S3). Greening and browning occurred with approximately equal frequency in evergreen needleleaf forest (18 [11, 22] % vs. 18 [16, 22] % of sample sites) (Figure 4c). There was a strong negative correlation between the intraclass prevalence of greening versus browning across land cover classes (r = −.92 [−.85, −.96]), such that land cover classes with a high prevalence of greening generally had low prevalence of browning and vice versa (Figure 4d).

3.4 | Vegetation greenness trends related to summer warmth

During the most recent 20 years, sample sites that greened had lower mean summer air temperatures (i.e., SWI) than sample sites that browned, both when pooling sample sites across the biome and within many individual land cover classes (Figure 5). The mean SWI from 2000 to 2019 averaged 53°C across sample sites, with 95% of sample sites having a mean SWI between 32 and 71°C (Figure 5a). For the whole biome, the cross-site average mean SWI was lowest at sample sites that greened (52 [50, 53]°C), intermediate at sample sites with no trend (55 [54.0, 56]°C), and highest

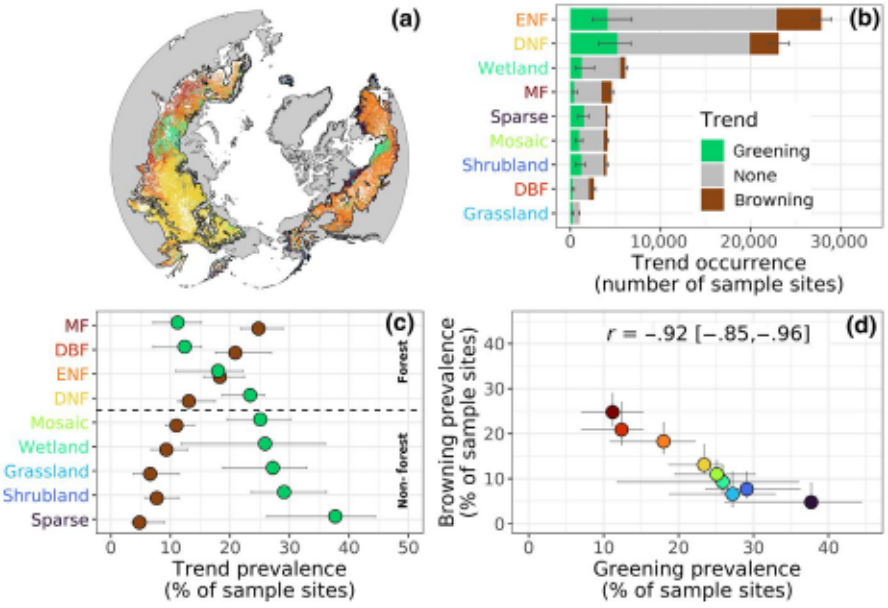

FIGURE 4 Vegetation greenness trends related to land cover class. (a) Distribution of land cover classes across the boreal forest. (b) Occurrence of sample sites in each land cover class where vegetation greenness significantly (= .10) increased (greening), decreased (browning), or had no trend (none) from 2000 to 2019 based on Mann–Kendall trend tests. (c) Prevalence of sample sites with recent greening or browning in each land cover class. (d) Comparison between the prevalence of greening and browning across land cover classes. Land cover classes include evergreen needleleaf forest (ENF), deciduous needleleaf forest (DNF), deciduous broadleaf forest (DBF), mixed forest (MF), and five colder nonforest classes. Note each land cover class is assigned a unique color that is consistently used. In (b) and (c), the land cover classes are ordered by total number of sample sites and prevalence of greening, respectively. Panels depict best estimates (bars, dots) and 95% confidence intervals derived from Monte Carlo simulations ($n = 10^3$). Land cover data from the European Space Agency's Climate Change Initiative Land Cover dataset (ESA, 2017)

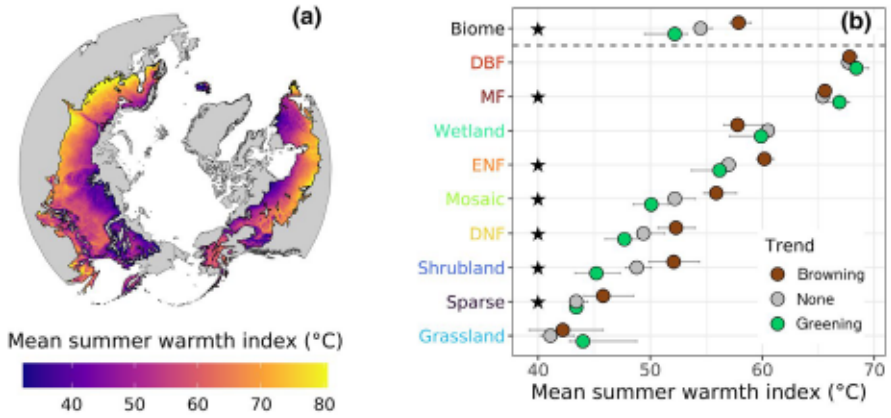

FIGURE 5 Vegetation greenness trends related to summer warmth by land cover class. (a) Mean summer warmth index (SWI) from 2000 to 2019 with SWI computed as the annual sum of mean monthly air temperatures above 0°C. The SWI is an indicator of total annual heat load. (b) Cross-site average of mean SWI for sample sites in each land cover class where vegetation greenness increased (greening), had no trend (none), or decreased (browning) from 2000 to 2019. Land cover classes are ordered from highest (top) to lowest (bottom) average mean SWI. Error bars are 95% confidence intervals derived from Monte Carlo simulations ($n = 10^3$). Black stars denote significant (= .05) differences in cross-site average of mean SWI between greening and browning classes based on permutation tests. The SWI was derived using TerraClimate data (Abatzoglou et al., 2018)

at sample sites that browned (58 [57, 59]°C). Permutation tests showed that average mean SWI was significantly (= .05) lower at sample sites that greened instead of browned not only for the overall biome but also for evergreen needleleaf forest, deciduous needleleaf forest, mosaic vegetation, shrublands, and sparse vegetation (Figure 5b). Mixed forest was the only land cover class where greening occurred at significantly higher average mean SWI than browning ($p = .03$).

3.5 | Environmental drivers of vegetation greenness trends

We assessed the degree to which recent changes in vegetation greenness were associated with climate, soil, and topography using Random Forest models. Specifically, these classification models attributed greening and browning classes from 2000 to 2019 with environmental predictors. Cross-validated model classification accuracy was 77 [74, 81] %, while the expected classification accuracy at random would be ~50% (Table S4). The six most important environmental predictors were mean annual SWI and soil temperature, followed by elevation and soil nitrogen content (0–5 cm depth), as well as changes in SWI and summer VPD from 2000 to 2019 (Figure 6a). Greening was most likely to occur at sample sites that had low summer air temperatures (i.e., SWI), cold soils, and high soil nitrogen, along with slightly increased summer air temperatures. Conversely, browning was most likely to occur at sample sites with high summer air temperatures, warm soils, and low soil nitrogen, along with increased summer air temperatures and VPD (Figure 6b). Greening was also more likely at low or high elevations, while browning was more likely at mid elevations.

4 | DISCUSSION

We evaluated changes in vegetation greenness during recent decades across the boreal forest biome using the Landsat satellites and found evidence supporting the hypothesis of an emerging biome shift associated with recent climate warming. Focusing on natural vegetation with low human pressure and no evidence of recent disturbance, we assessed changes in vegetation greenness using an ensemble of cross-calibrated and phenologically harmonized vegetation indices derived from moderate resolution Landsat measurements in a Monte Carlo uncertainty framework. We found an overall increase in median pan-boreal vegetation greenness with greening being 1.5–3.0 times more common than browning, depending on period. Greening primarily occurred in cold sparsely treed areas with high soil nitrogen and moderate summer warming, whereas browning was concentrated in warm densely treed areas where summer temperatures and VPD increased. Landsat observations of vegetation greenness have been linked to field measurements of vegetation productivity and mortality in boreal and tundra ecosystems (Table 2). Our study thus contributes to mounting evidence from field and remote sensing studies showing vegetation changes in the northern (Beck et al., 2011; Esper & Schweingruber, 2004; Frost & Epstein, 2014; Lantz et al., 2019; Rees et al., 2020) and southern (Beck et al., 2011; Kharuk et al., 2020; Kukavskaya et al., 2016) ecotones of the boreal forest that indicate a biome shift is indeed underway, albeit not uniformly across these expansive ecotones. Large-scale vegetation changes over coming decades could have manifold implications for biodiversity, hydrology, permafrost, climate feedbacks, and communities across the high northern latitudes.

While median vegetation greenness of recently undisturbed areas increased during the past four decades in the boreal forest, we found a potential slowdown in the rate of increase during the last

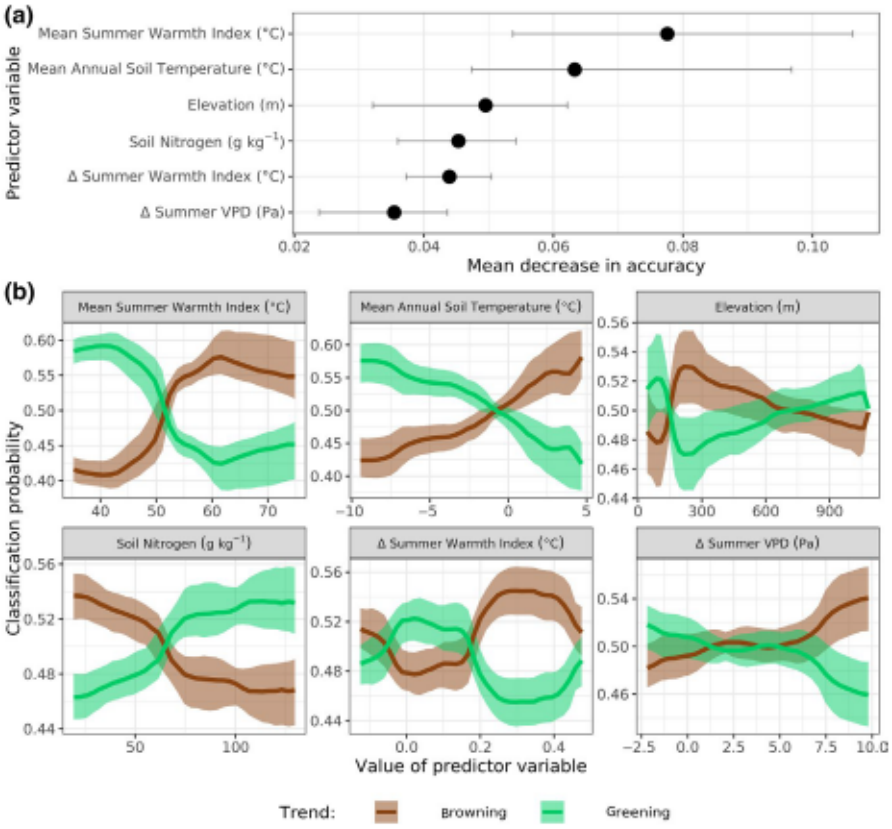

FIGURE 6 Environmental predictors of recent greening and browning. Random Forest models predicted with 77 [74, 81] % accuracy whether samples sites significantly (= .10) greened or browned from 2000 to 2019 based on environmental predictors. (a) Variable importance of the six most important predictors as quantified by the mean decrease in accuracy, where a higher value indicates greater importance to classification accuracy. (b) Partial dependency plots show how classification probability varies with each predictor while holding all other predictors in the model at their average value. Climate means and changes (Δ for SWI and VPD) were for the period 2000–2019, except for mean annual soil temperature which was for the period 2000–2016 given available data. The panels depict best estimates (dots or lines) and 95% confidence intervals (whiskers or bands) derived from Monte Carlo simulations ($n = 10^3$)

two decades. Specifically, median vegetation greenness increased at a rate of 0.15 [0.06, 0.22] % yr^{-1} from 1985 to 2019, but at a rate of 0.07 [−0.06, 0.14] % yr^{-1} from 2000 to 2019. These multidecadal changes in vegetation greenness suggest an increase in peak summer productivity that broadly aligns with enhanced summer carbon uptake inferred from atmospheric inversions (Lin et al., 2020; Welp et al., 2016), land surface modeling (Forkel et al., 2016), and coarse resolution satellite observations (Beck & Goetz, 2011; Park et al., 2016). Increasing productivity is likely due to warmer and longer growing seasons (Forkel et al., 2016; Piao et al., 2020), higher nutrient availability from permafrost thaw (Peng et al., 2020), and expansion of trees and shrubs in the forest–tundra ecotone (Forkel et al., 2016; Frost & Epstein, 2014), with CO_2 fertilization playing a minor role (Girardin et al., 2016; Piao et al., 2020). Nevertheless, ongoing warming has reduced the extent to which low temperatures limit tree growth (Babst et al., 2019) and vegetation canopy cover (Keenan & Riley, 2018) across parts of the southern boreal forest. This could explain the reduced rate of greening during the last two decades and challenges ecosystem models to better account for how boreal forest productivity and carbon balance will respond to warming (IPCC, 2021) with more extreme heatwaves (Perkins-Kirkpatrick & Gibson, 2017) and droughts (Cook et al., 2020) over the next few decades.

Our Landsat analysis broadly supports changes detected using coarse resolution AVHRR NDVI (Guay et al., 2014; Park et al., 2016), but also highlights discrepancies between these satellite records that are at least partly a result of increased spatial resolution. Our higher resolution assessment corroborates greening in sparse forests and browning in denser forests (Beck & Goetz, 2011), but showed somewhat less greening (38 [29, 42] % vs ~44%) and considerably more browning (13 [9, 15] % vs. ~2%) than a recent assessment with AVHRR NDVI (Park et al., 2016). Some of these differences may also be related to the period and spatial domain analyzed, as well as various vegetation indices used. Nevertheless, our findings align with recent analyses from the Arctic tundra biome (Berner et al., 2020) and northern North America (Ju & Masek, 2016). In the boreal forest, patches of greening, browning, and stable vegetation can occur in close proximity (Ju & Masek, 2016; Wang & Friedl, 2019); thus, coarse resolution AVHRR NDVI likely inflates the extent of greening given enough greening hotspots in landscapes with otherwise stable vegetation. Similarly, AVHRR NDVI likely fails to detect patches of browning in landscapes with mostly stable or greening vegetation (Berner et al., 2020; Myers-Smith et al., 2020). Landsat's far higher spatial resolution makes it more suited for monitoring and understanding the types, extents, and drivers of heterogeneous ecological changes in the boreal forest (Pastick et al., 2019; Sulla-Menashe et al., 2017; Wang et al., 2021), although cross-sensor calibration and phenological harmonization are still necessary for consistent use of these data (Berner et al., 2020; Ju & Masek, 2016).

We further show widespread greening occurred in the cold margins of the boreal forest during the past several decades. Specifically, we found greening at 22–38% of sample sites that were concentrated in sparse conifer forests with low summer air and annual soil temperatures, as well as in colder tundra land cover classes (e.g., shrublands). Regional studies have documented increasing growth, cover, and/or density of trees and shrubs in regions where we detected extensive greening such as the Labrador Peninsula

TABLE 2 Summary of recent studies relating Landsat NDVI to field measurements of vegetation dynamics and structure in boreal forest and tundra ecosystems. Temporal or spatial relationships were characterized with Pearson's correlations (r), Spearman's correlations (r_s), nonlinear regression (r^2), and mixed-effect models (marginal r^2)

Field data	Main result	Reference
Ecosystem productivity	Tundra gross primary productivity was positively correlated with spatial variation in $NDVI_{max}$ across 11 eddy covariance flux towers in three Arctic countries ($r_s = .72$)	Berner et al. (2020)
Forest productivity	Trembling aspen (*Populus tremuloides*) stand productivity was positively associated with temporal variation in $NDVI_{max}$ at 22 field sites in the Alaskan boreal forest (marginal $r^2 = .66$ with mortality rate as significant covariate)	Boyd et al. (2021)
	Cajander larch (*Larix cajanderi*) stand productivity was positively associated with temporal variation in $NDVI_{max}$ at 19 field sites in the Siberian boreal forest–tundra ecotone (marginal $r^2 = .09–.28$ depending on stand density)	Walker et al. (2021)
Tree growth	Trembling aspen (*Populus tremuloides*) growth was positively associated with temporal variation in $NDVI_{max}$ at 22 field sites in the Alaskan boreal forest (marginal $r^2 = .27$)	Boyd et al. (2021)
	Trembling aspen (*Populus tremuloides*) growth was positively associated with temporal variation in $NDVI_{July–August}$ at four field sites in the Alaskan boreal forest (marginal $r^2 = .23$)	Boyd et al. (2019)
	Siberian larch (*Larix siberica*) growth was positively correlated with temporal variation in $NDVI_{max}$ at 13 of 15 field sites in the Mongolian boreal forest–steppe ecotone (median $r = .60$)	Erasmi et al. (2021)
Shrub growth	Deciduous shrub growth was positively correlated with temporal variation in $NDVI_{max}$ at 19 of 22 field sites in six Arctic countries (median $r_s = .42$)	Berner et al. (2020)
	Dwarf birch (*Betula glandulosa*) growth was positively correlated with temporal variation in $NDVI_{July–August}$ at a field site in the Canadian Arctic ($r_s = .60$)	Davis et al. (2020)
Aboveground biomass	Tundra and shrub aboveground biomass were positively associated with spatial variation in $NDVI_{max}$ across 28 field sites in the Alaskan and Canadian Arctic ($r^2 = .79$ and $r^2 = .82$, respectively)	Berner et al. (2018)
	Tundra aboveground biomass was positively associated with spatial variation in $NDVI_{August}$ across 104 field sites in the Norwegian Arctic ($r^2 = .68$)	Johansen and Tømmervik (2014)
Vegetation mortality	Trembling aspen (*Populus tremuloides*) stand mortality was negatively associated with temporal variation in $NDVI_{max}$ at 22 field sites in the Alaskan boreal forest (marginal $r^2 = .66$ with productivity as a significant covariate)	Boyd et al. (2021)
	Tree mortality events were associated with negative trends and anomalies in $NDVI_{July–August}$ across regional networks of field sites ($n > 760$) in the Alaskan and Canadian boreal forest	Rogers et al. (2018)
	Massive landslides killed nearly all tundra vegetation and caused $NDVI_{July–August}$ to decrease ~45% across disturbed areas in the West Siberian Arctic	Verdonen et al. (2020)

(Canada) (Ropars et al., 2015; Trant & Hermanutz, 2014), Northwest Territories (Canada) (Lantz et al., 2013, 2019), and Western Siberia (Russia) (Devi et al., 2008; Esper & Schweingruber, 2004; Frost & Epstein, 2014). In Western Siberia, tree-ring measurements from nine field sites showed increased growth and recruitment of larch (*Larix* spp.), Siberian pine (*Pinus sibirica*), and Siberian spruce (*Picea obovata*) in the forest–tundra ecotone during periods of decadal warming in the 1940–1950s and since the early 1970s (Esper & Schweingruber, 2004). In cold northern regions, higher summer temperatures can increase tree and shrub growth (Andreu-Hayles et al., 2020; Hellmann et al., 2016; Ropars et al., 2015), lead to the production of more viable seeds (Lantz et al., 2010, 2019), and promote seedling recruitment (Esper & Schweingruber, 2004; Kharuk et al., 2013; Wieczorek et al., 2017) that can drive infilling (Lantz et al., 2019; Wieczorek et al., 2017) and gradual northward and upslope migration of trees and shrubs into herbaceous tundra (Esper & Schweingruber, 2004; Kharuk et al., 2013; Myers-Smith & Hik, 2018; Rees et al., 2020; Trant & Hermanutz, 2014). Thermal regimes restrict the locations of Arctic and alpine treelines (Maher et al., 2021; Paulsen & Körner, 2014), but tree migration into tundra has not kept

pace with recent warming (Rees et al., 2020) likely because migration is constrained by seed dispersal, seedling herbivory, and other factors such as pathogens, snow cover, and cold, nutrient-poor permafrost soils that are buffered from climate warming (Van Bogaert et al., 2011; Maher et al., 2021; Olnes et al., 2017; Rees et al., 2020; Stöcklin & Körner, 1999). Greening in recent decades is linked to climate warming increasing growth, biomass, and probably recruitment of trees and shrubs in a significant portion of the forest–tundra ecotone, but such changes have not occurred everywhere along the cold margins of the boreal forest (Rees et al., 2020; Timoney et al., 2019).

Earth's atmosphere is now warming more rapidly than it has in at least the last ~2,000 years (IPCC, 2021), yet most sample sites in our analysis exhibited no systematic trend in vegetation greenness during the last four decades. This was especially true not only of sample sites within the climatically central portions of the boreal forest biome but also within the central portions of the primary forest types (i.e., evergreen and deciduous needleleaf forests). Forests in these core areas may be more resilient to change until some climatic threshold is surpassed (Chapin et al., 2004). Moreover, climate warming may not increase vegetation greenness or productivity if access to soil nutrients or water constrains physiological processes like photosynthesis or growth (Berner et al., 2013; Ellison et al., 2019; Foster et al., 2019) nor might warming decrease vegetation productivity in water-limited regions if greater evaporative demands are offset by higher water use efficiency from CO_2 fertilization (Sullivan et al., 2017). Our finding that greening was more probable where there was high soil nitrogen provides further support for the role of soil nutrients in mediating vegetation response to warming. Tree growth response to warming can also be mediated by the intensity of intra-stand competition for soil nutrients (Foster et al., 2019; Walker et al., 2021). It is also likely that important ecological responses to climate change could be occurring in areas where remotely sensed metrics of vegetation greenness show no long-term trend. For example, spruce or larch recruitment might minimally affect vegetation greenness in shrubby landscapes (Huemmrich et al., 2021; Loranty et al., 2018), as might low levels of tree mortality where the growth of surviving trees is enhanced by reduced competition (Boyd et al., 2021). To better understand variability in boreal forest resilience to future climatic changes, it will be necessary to further develop and apply mechanistic ecological models that simulate species-specific responses to changes at fine spatial scales (Foster et al., 2019).

Browning primarily occurred in the climatically warmest margins of both the boreal forest biome and major forest types, especially where summers became warmer and drier. This observation is consistent with field measurements in many such locations. For example, we detected browning in eastern interior Alaska where long-term ecological research has documented declining tree growth and browning associated with warming-induced drought stress and insect outbreaks (Barber et al., 2000; Beck et al., 2011; Boyd et al., 2021; Juday & Alix, 2012; Parent & Verbyla, 2010). However, a recent study from this region found little evidence of growth declines in black spruce (*P. mariana*) or white spruce (*P. glauca*) during recent decades and instead suggested rising concentrations of atmospheric CO_2 could have stabilized growth by compensating for increasing evaporative demand (Sullivan et al., 2017). Local to regional variability is evident in the boreal biome, which has not exhibited widespread response to CO_2 fertilization (Girardin et al., 2016). We also detected browning in larch forests on the eastern Central Siberian Plateau, where hot and dry summers cause forest carbon uptake to be very sensitive to high summer VPD (Dolman et al., 2004) and declines in tree growth have been reported (Hellmann et al., 2016). In addition to declining tree growth, browning is also likely related to increasing rates of tree mortality linked with warming-induced drought stress along the warm dry margins of the boreal forest in North America (Michaelian et al., 2011; Peng et al., 2011; Refsland & Cushman, 2021; Rogers et al., 2018) and Eurasia (Allen et al., 2015; Kharuk et al., 2020). In boreal North America, annual rates of tree mortality approximately doubled since the 1980s and are especially high in trembling aspen (*Populus tremuloides*) (Peng et al., 2011; Refsland & Cushman, 2021; Rogers et al., 2018), which aligns with our finding that browning was particularly prevalent in deciduous broadleaf forests (e.g., aspen). Overall, drawing on spatially comprehensive and current remote sensing datasets, our analysis shows recent browning in the climatically warmest parts of the boreal forest biome where rising summer temperatures and VPD have been linked with reduced tree growth and increased tree mortality. These changes in forest greenness, growth, and mortality could foreshadow warming-induced transitions of dense forests toward patches of woodland, shrubland, and grassland along the warm climatic margins of the boreal forest.

Disturbance and subsequent succession can cause pronounced multidecadal changes in vegetation greenness that complicate efforts to detect early indicators of a biome shift using satellite remote sensing (Fiore et al., 2020; Sulla-Menashe et al., 2017). Pulse disturbance events (e.g., wildfire, harvest) lead vegetation greenness to abruptly decrease, followed by a gradual increase over the subsequent two to four decades of succession (Beck & Goetz, 2011; Fiore et al., 2020; Sulla-Menashe et al., 2017). To alleviate these effects, we focused on areas of naturally occurring vegetation with low human pressure (Venter et al., 2016) that were nominally free from harvest, wildfire, and other disturbances since at least the early 1980s (Giglio et al., 2018; Guindon et al., 2017; Hansen et al., 2013; Loboda & Chen, 2017). However, we likely did not manage to exclude all disturbances after the early 1980s owing to errors of omission in the underlying disturbance datasets, yet such residual disturbances were less probable during the post-2000 period given extensive efforts to map contemporary disturbances (Giglio et al., 2018; Hansen et al., 2013). Vegetation recovery after disturbance in the 1960s and 1970s contributed to some of the greening we observed, especially from 1985 to 2019, yet it was not possible to consistently exclude disturbances from these earlier decades because comparable spatial information was not available. Therefore, we primarily focused on vegetation greenness trends from 2000 to 2019 that likely were less influenced by residual disturbances and post-disturbance recovery (Fiore et al., 2020; Sulla-Menashe et al., 2017) and have better

geographic coverage than earlier periods due to greater availability of Landsat data. It is unlikely the observed greening and browning trends were primarily due to disturbance and succession given both our efforts to exclude recent disturbances and the distinct bioclimatic settings where these spectral trends occurred. Rather, these greening and browning trends likely reflect underlying shifts in vegetation productivity, mortality, and recruitment arising from mounting impacts of rapid climatic changes on the northernmost forest biome.

To detect early indicators of a boreal biome shift, we focused on vegetation greenness trends in recently undisturbed areas; however, increasing wildfire activity could play an important role catalyzing a biome shift (Baltzer et al., 2021; Kukavskaya et al., 2016; Stralberg et al., 2018; Tchebakova et al., 2009). In recent decades, warmer and drier conditions contributed to increasing wildfire activity in boreal North America (Walker et al., 2020) and Eurasia (Kharuk et al., 2021; Kukavskaya et al., 2016). In both continents, boreal forest conversion to woodlands, shrublands, or grasslands has been document after recent wildfires, particularly in warm and dry regions (Baltzer et al., 2021; Kukavskaya et al., 2016) such as the southern margin of the boreal forest in Siberia that borders grassland steppe (Barrett et al., 2020; Kukavskaya et al., 2016). Forests can lose resilience to wildfire when shorter fire return intervals reduce seed availability and more frequent postfire droughts reduce seedling establishment, both contributing to tree regeneration failure (Baltzer et al., 2021; Kukavskaya et al., 2016; Whitman et al., 2019). Conversely, increasing wildfire activity could facilitate forest expansion into Arctic tundra (Alexander et al., 2018; Lloyd et al., 2007). Near treeline in far northeastern Siberia, a recent experiment showed that Cajander larch (*L. cajanderi*) recruitment was much higher in burned than unburned plots and increased with burn severity because of improved seedbed conditions associated with soils that were warmer, wetter, and had thinner organic layers (Alexander et al., 2018). Wildfire activity is expected to increase with continued warming over the coming century and will contribute to further vegetation shifts along the southern and northern margins of the boreal forest (Gonzalez et al., 2010; Stralberg et al., 2018; Tchebakova et al., 2009).

Boreal forest greening and browning trends have typically been quantified using NDVI (e.g., Beck & Goetz, 2011; Myneni et al., 1997; Sulla-Menashe et al., 2017), whereas here we quantified these trends using an ensemble of vegetation indices that included NDVI and three newer metrics (i.e., EVI2, NIRv, and kNDVI). Changes in Landsat NDVI have been linked with spatial or temporal variation in ecosystem productivity, forest productivity, tree growth, shrub growth, aboveground biomass, and vegetation mortality at field sites in high northern latitudes (Table 2). However, Landsat NDVI can saturate in dense forests, likely hindering detection of greening and biasing observed trends toward browning under such conditions (Huemmrich et al., 2021). We therefore also used three newer vegetation indices that are likely less prone to saturation and better indicators of vegetation dynamics, though their performance has not been thoroughly evaluated in high northern latitudes (Badgley et al., 2017; Camps-Valls et al., 2021; Jiang et al., 2008). We focus on results derived using the ensemble of vegetation indices but note that NDVI and kNDVI detected ~30% less greening and ~30% more browning than EVI2 and NIRv (Table S2), underscoring differences among vegetation indices. To guide future assessments of greening and browning in boreal and tundra ecosystems, further field validations are needed for newer vegetation indices.

In conclusion, by drawing on moderate resolution Landsat satellite observations, we show that there have been systematic trends in vegetation greenness during recent decades that are consistent with an emerging boreal biome shift associated with ongoing climate warming. Climate warming contributed to greening in the cool forest–tundra ecotone but browning in the warm southern margins of the boreal forest, though there was little to no systematic change in vegetation greenness across much of the biome. Long-term trends in vegetation greenness reflect underlying shifts in growth, recruitment, and mortality of trees, shrubs, and other vegetation; however, remotely sensed metrics of vegetation greenness do not fully capture the extent of ecosystem changes associated with climate warming and shifts in water availability. Hence, to better understand the extent, causes, and consequences of a boreal biome shift, it will be essential to expand ground-based ecological monitoring, advance mechanistic ecosystem models, and further capitalize on satellite remote sensing assets like Landsat for improved mapping of forest extent, composition, and disturbance dynamics in recent decades. Improved monitoring will be especially important over the next few decades given projections of accelerated warming with increasing extreme events (e.g., heatwaves, droughts, and mega-fires) that could drive rapid and potentially unanticipated changes in the boreal forest. Our analysis provides evidence of extensive climatically linked vegetation changes along the warm and cool margins of the boreal forest biome that will have broad ecological and societal implications.

ACKNOWLEDGMENTS

We thank the many researchers who generated and made publicly available the spatial datasets that we used in this study. We also thank two anonymous reviewers whose feedback helped improve this paper. This study was supported by the National Aeronautics and Space Administration (NASA) Arctic Boreal Vulnerability Experiment (ABoVE) and NASA Carbon Cycle Science grants NNX17AE44G, 80NSSC19M0112, and NNX17AE13G to SJG. Computational analyses were performed on Northern Arizona University's Monsoon computing cluster that is funded by Arizona's Technology and Research Initiative Fund. Authors declare that they have no competing interests.

AUTHOR CONTRIBUTIONS

The study was designed by LTB and SJG; analyses and visualizations were performed by LTB; and writing was led by LTB with contributions from SJG. Funding for the research was acquired by SJG.

CODE AVAILABILITY

All code from this analysis is publicly archived in a GitHub repository (https://github.com/logan-berner/boreal_biome_shift).

DATA AVAILABILITY STATEMENT

The datasets generated as part of this study are publicly available through the Oak Ridge National Laboratory (ORNL) Distributed Active Archive Center (DAAC) for Biogeochemical Dynamics (Berner & Goetz, 2022). The analysis also relied on datasets from the following sources: The Terrestrial Ecoregions of the World dataset is available from the World Wildlife Fund (https://www.worldwildlife.org/publications/terrestrial-ecoregions-of-the-world). The Landsat surface reflectance data are available from the United States Geological Survey (USGS) through Google Earth Engine (GEE; https://earthengine.google.com/). The Ecological Land Units dataset is available from the USGS (https://www.usgs.gov/centers/gecsc/science/global-ecosystems). The Global Multi-resolution Terrain Elevation Data (GMTED) are available from the USGS and National Geospatial Agency (NGA) through GEE. The MODIS burned area and tree cover datasets are available from NASA through GEE. The Human Footprint Index dataset is available from NASA's Socioeconomic Data and Applications Center (SEDAC) (https://sedac.ciesin.columbia.edu/data/set/wildareas-v2-human-footprint-geographic/data-download). The Russian Young Forests dataset is available from the ORNL DAAC (https://daac.ornl.gov/cgi-bin/dsviewer.pl?ds_id=1330). The Climate Change Initiative 2 (CCI2) Global Land Cover dataset is available from the European Space Agency (http://www.esa-landcover-cci.org). The Canadian Landsat Disturbance (CanLad) 2017 dataset is available from the Government of Canada (https://open.canada.ca/data/en/dataset/add1346b-f632-4eb9-a83d-a662b38655ad). The Global Forest Change dataset is available from the University of Maryland through GEE. The TerraClimate dataset is available from the University of Idaho (http://www.climatologylab.org/terraclimate.html). The SoilGrids soil nitrogen dataset is available from the International Soil Reference and Information Centre, (https://www.isric.org/explore/soilgrids). The Ground Temperature Map, 2000–2016, Northern Hemisphere Permafrost dataset is available from the Hemholtz Centre for Polar and Marine Research through PANGAEA (https://doi.org/10.1594/PANGAEA.888600).

ORCID

Logan T. Berner https://orcid.org/0000-0001-8947-0479
Scott J. Goetz https://orcid.org/0000-0002-6326-4308

REFERENCES

Abatzoglou, J. T., Dobrowski, S. Z., Parks, S. A., & Hegewisch, K. C. (2018). TerraClimate, a high-resolution global dataset of monthly climate and climatic water balance from 1958–2015. *Scientific Data*, *5*, 1958–2015. https://doi.org/10.1038/sdata.2017.191

Alexander, H. D., Natali, S. M., Loranty, M. M., Ludwig, S. M., Spektor, V. V., Davydov, S., Zimov, N., Trujillo, I., & Mack, M. C. (2018). Impacts of increased soil burn severity on larch forest regeneration on permafrost soils of far northeastern Siberia. *Forest Ecology and Management*, *417*, 144–153. https://doi.org/10.1016/j.foreco.2018.03.008

Allen, C. D., Breshears, D. D., & McDowell, N. G. (2015). On underestimation of global vulnerability to tree mortality and forest die-off from hotter drought in the Anthropocene. *Ecosphere*, *6*(8), 1–55. https://doi.org/10.1890/ES15-00203.1

Andreu-Hayles, L., Gaglioti, B. V., Berner, L. T., Levesque, M., Anchukaitis, K. J., Goetz, S. J., & D'Arrigo, R. (2020). A narrow window of summer temperatures associated with shrub growth in Arctic Alaska. *Environmental Research Letters*, *15*, 105012. https://doi.org/10.1088/1748-9326/ab897f

Aybar, C., Wu, Q., Bautista, L., Yali, R., & Barja, A. (2020). rgee: An R package for interacting with Google Earth Engine. *Journal of Open Source Software*, *5*(51), 2272. https://doi.org/10.21105/joss.02272

Babst, F., Bouriaud, O., Poulter, B., Trouet, V., Girardin, M. P., & Frank, D. C. (2019). Twentieth century redistribution in climatic drivers of global tree growth. *Science Advances*, *5*(1), eaat4313. https://doi.org/10.1126/sciadv.aat4313

Badgley, G., Field, C. B., & Berry, J. A. (2017). Canopy near-infrared reflectance and terrestrial photosynthesis. *Science Advances*, *3*(3), e1602244. https://doi.org/10.1126/sciadv.1602244

Baltzer, J. L., Day, N. J., Walker, X. J., Greene, D., Mack, M. C., Alexander, H. D., Arseneault, D., Barnes, J., Bergeron, Y., Boucher, Y., Bourgeau-Chavez, L., Brown, C. D., Carrière, S., Howard, B. K., Gauthier, S., Parisien, M.-A., Reid, K. A., Rogers, B. M., Roland, C., … Johnstone, J. F. (2021). Increasing fire and the decline of fire adapted black spruce in the boreal forest. *Proceedings of the National Academy of Sciences*, *118*(45), e2024872118. https://doi.org/10.1073/pnas.2024872118

Barber, V. A., Juday, G. P., & Finney, B. P. (2000). Reduced growth of Alaskan white spruce in the twentieth century from temperature-induced drought stress. *Nature*, *405*(6787), 668–673.

Barrett, K., Baxter, R., Kukavskaya, E., Balzter, H., Shvetsov, E., & Buryak, L. (2020). Postfire recruitment failure in Scots pine forests of southern Siberia. *Remote Sensing of Environment*, *237*, 111539. https://doi.org/10.1016/j.rse.2019.111539

Beck, P. S. A., & Goetz, S. J. (2011). Satellite observations of high northern latitude vegetation productivity changes between 1982 and 2008: ecological variability and regional differences. *Environmental Research Letters*, *6*(4). https://doi.org/10.1088/1748-9326/6/4/045501

Beck, P. S. A., Juday, G. P., Alix, C., Barber, V. A., Winslow, S. E., Sousa, E. E., Heiser, P., Herriges, J. D., & Goetz, S. J. (2011). Changes in forest productivity across Alaska consistent with biome shift. *Ecology Letters*, *14*(4), 373–379. https://doi.org/10.1111/j.1461-0248.2011.01598.x

Berner, L. T., Assmann, J. J., Normand, S., & Goetz, S. J. (2022). lsatTS - an R package for deriving vegetation greenness time series using Landsat satellite data. https://github.com/logan-berner/lsatTS

Berner, L. T., Beck, P. S. A., Bunn, A. G., & Goetz, S. J. (2013). Plant response to climate change along the forest-tundra ecotone in northeastern Siberia. *Global Change Biology*, *19*(11), 3449–3462. https://doi.org/10.1111/gcb.12304

Berner, L. T., & Goetz, S. J. (2022). ABoVE: landsat vegetation greenness trends, boreal forest biome, 1985–2019. *ORNL Distributed Active Archive Center*, https://doi.org/10.3334/ORNLDAAC/2023

Berner, L. T., Jantz, P., Tape, K. D., & Goetz, S. J. (2018). Tundra plant aboveground biomass and shrub dominance mapped across the North Slope of Alaska. *Environmental Research Letters*, *13*(3). https://doi.org/10.1088/1748-9326/aaaa9a

Berner, L. T., Massey, R., Jantz, P., Forbes, B. C., Macias-Fauria, M., Myers-Smith, I., Kumpula, T., Gauthier, G., Andreu-Hayles, L., Gaglioti, B. V., Burns, P., Zetterberg, P., D'Arrigo, R., & Goetz, S. J. (2020). Summer warming explains widespread but not uniform greening in

the Arctic tundra biome. *Nature Communications*, *11*, 4621. https://doi.org/10.1038/s41467-020-18479-5

Bonan, G. B. (2008). Forests and climate change: forcings, feedbacks, and the climate benefits of forests. *Science*, *320*(5882), 1444–1449. https://doi.org/10.1126/science.1155121

Boyd, M. A., Berner, L. T., Doak, P., Goetz, S. J., Rogers, B. M., Wagner, D., Walker, X. J., & Mack, M. C. (2019). Impacts of climate and insect herbivory on productivity and physiology of trembling aspen (Populus tremuloides) in Alaskan boreal forests. *Environmental Research Letters*, *14*(8). https://doi.org/10.1088/1748-9326/ab215f

Boyd, M. A., Berner, L. T., Foster, A. C., Goetz, S. J., Rogers, B. M., Walker, X. J., & Mack, M. C. (2021). Historic declines in growth portend trembling aspen death during a contemporary leaf miner outbreak in Alaska. *Ecosphere*, *12*(6), e03569. https://doi.org/10.1002/ecs2.3569

Bradshaw, C. J., & Warkentin, I. G. (2015). Global estimates of boreal forest carbon stocks and flux. *Global and Planetary Change*, *128*, 24–30. https://doi.org/10.1016/j.gloplacha.2015.02.004

Breiman, L. (2001). Random forests. *Machine Learning*, *45*, 5–32.

Bronaugh, D., & Werner, A. (2019). zyp: Zhang + Yue-Pilon trends package. R package version 0.10-1.1. https://CRAN.R-project.org/package=zyp

Bunn, A. G., & Goetz, S. J. (2006). Trends in satellite-observed circumpolar photosynthetic activity from 1982 to 2003: the influence of seasonality, cover type, and vegetation density. *Earth Interactions*, *10*, 1–19. https://doi.org/10.1175/EI190.1

Camps-Valls, G., Campos-Taberner, M., Moreno-Martínez, Á., Walther, S., Duveiller, G., Cescatti, A., Mahecha, M. D., Muñoz-Marí, J., García-Haro, F. J., Guanter, L., Jung, M., Gamon, J. A., Reichstein, M., & Running, S. W. (2021). A unified vegetation index for quantifying the terrestrial biosphere. *Science Advances*, *7*(9), eabc7447. https://doi.org/10.1126/sciadv.abc7447

Chapin, F. S., Callaghan, T. V., Bergeron, Y., Fukuda, M., Johnstone, J., Juday, G., & Zimov, S. (2004). Global change and the boreal forest: thresholds, shifting states or gradual change? *AMBIO: A Journal of the Human Environment*, *33*(6), 361–366. https://doi.org/10.1579/0044-7447-33.6.361

Cook, B., Mankin, J., Marvel, K., Williams, A., Smerdon, J., & Anchukaitis, K. (2020). Twenty-first century drought projections in the CMIP6 forcing scenarios. *Earth's Future*, *8*(6), e2019EF001461. https://doi.org/10.1029/2019EF001461

Danielson, J. J., & Gesch, D. B. (2011). Global multi-resolution terrain elevation data 2010 (GMTED2010): US Department of the Interior, US Geological Survey.

Davis, E., Trant, A., Hermanutz, L., Way, R. G., Lewkowicz, A. G., Collier, L. S., & Whitaker, D. (2020). Plant-environment interactions in the low arctic torngat mountains of labrador. *Ecosystems*, *24*, 1038–1058.

Devi, N., Hagedorn, F., Moiseev, P., Bugmann, H., Shiyatov, S., Mazepa, V., & Rigling, A. (2008). Expanding forests and changing growth forms of Siberian larch at the Polar Urals treeline during the 20th century. *Global Change Biology*, *14*(7), 1581–1591. https://doi.org/10.1111/j.1365-2486.2008.01583.x

Dial, R. J., Berg, E. E., Timm, K., McMahon, A., & Geck, J. (2007). Changes in the alpine forest-tundra ecotone commensurate with recent warming in southcentral Alaska: Evidence from orthophotos and field plots. *Journal of Geophysical Research: Biogeosciences*, *112*, G04015. https://doi.org/10.1029/2007JG000453

DiMiceli, C., Townshend, J., Carroll, M., & Sohlberg, R. (2021). Evolution of the representation of global vegetation by vegetation continuous fields. *Remote Sensing of Environment*, *254*, 112271. https://doi.org/10.1016/j.rse.2020.112271

Dolman, A., Maximov, T., Moors, E., Maximov, A., Elbers, J., Kononov, A., & Van der Molen, M. (2004). Net ecosystem exchange of carbon dioxide and water of far eastern Siberian Larch (*Larix cajanderii*) on permafrost. *Biogeosciences*, *1*(2), 133–146.

Dowle, M., & Srinivasan, A. (2021). data.table: Extension of `data.frame`. R package version 1.14.2. https://CRAN.R-project.org/package=data.table

Ellison, S. B., Sullivan, P. F., Cahoon, S. M., & Hewitt, R. E. (2019). Poor nutrition as a potential cause of divergent tree growth near the Arctic treeline in northern Alaska. *Ecology*, *100*(12), e02878. https://doi.org/10.1002/ecy.2878

Erasmi, S., Klinge, M., Dulamsuren, C., Schneider, F., & Hauck, M. (2021). Modelling the productivity of Siberian larch forests from Landsat NDVI time series in fragmented forest stands of the Mongolian forest-steppe. *Environmental Monitoring and Assessment*, *193*(4), 1–18. https://doi.org/10.1007/s10661-021-08996-1

ESA (2017). Land Cover CCI Product User Guide Version 2. Tech. Rep. Available at: maps.elie.ucl.ac.be/CCI/viewer/download/ESACCI-LC-Ph2-PUGv2_2.0.pdf

Esper, J., & Schweingruber, F. H. (2004). Large-scale treeline changes recorded in Siberia. *Geophysical Research Letters*, *31*(6), L06202. https://doi.org/10.1029/2003GL019178

Fiore, N. M., Goulden, M. L., Czimczik, C. I., Pedron, S. A., & Tayo, M. A. (2020). Do recent NDVI trends demonstrate boreal forest decline in Alaska? *Environmental Research Letters*, *15*(9). https://doi.org/10.1088/1748-9326/ab9c4c

Forkel, M., Carvalhais, N., Rödenbeck, C., Keeling, R., Heimann, M., Thonicke, K., & Reichstein, M. (2016). Enhanced seasonal CO2 exchange caused by amplified plant productivity in northern ecosystems. *Science*, *351*(6274), 696–699.

Forkel, M., Carvalhais, N., Verbesselt, J., Mahecha, M., Neigh, C., & Reichstein, M. (2013). Trend change detection in NDVI time series: effects of inter-annual variability and methodology. *Remote Sensing*, *5*(5), 2113. https://doi.org/10.3390/rs5052113

Foster, A. C., Armstrong, A. H., Shuman, J. K., Shugart, H. H., Rogers, B. M., Mack, M. C., Goetz, S. J., & Ranson, K. J. (2019). Importance of tree- and species-level interactions with wildfire, climate, and soils in interior Alaska: Implications for forest change under a warming climate. *Ecological Modelling*, *409*, 108765. https://doi.org/10.1016/j.ecolmodel.2019.108765

Frost, G. V., & Epstein, H. E. (2014). Tall shrub and tree expansion in Siberian tundra ecotones since the 1960s. *Global Change Biology*, *20*(4), 1264–1277. https://doi.org/10.1111/gcb.12406

Giglio, L., Boschetti, L., Roy, D. P., Humber, M. L., & Justice, C. O. (2018). The Collection 6 MODIS burned area mapping algorithm and product. *Remote Sensing of Environment*, *217*, 72–85. https://doi.org/10.1016/j.rse.2018.08.005

Girardin, M. P., Bouriaud, O., Hogg, E. H., Kurz, W., Zimmermann, N. E., Metsaranta, J. M., & Büntgen, U. (2016). No growth stimulation of Canada's boreal forest under half-century of combined warming and CO2 fertilization. *Proceedings of the National Academy of Sciences*, *113*(52), E8406–E8414.

Gonzalez, P., Neilson, R. P., Lenihan, J. M., & Drapek, R. J. (2010). Global patterns in the vulnerability of ecosystems to vegetation shifts due to climate change. *Global Ecology and Biogeography*, *19*(6), 755–768. https://doi.org/10.1111/j.1466-8238.2010.00558.x

Gorelick, N., Hancher, M., Dixon, M., Ilyushchenko, S., Thau, D., & Moore, R. (2017). Google earth engine: Planetary-scale geospatial analysis for everyone. *Remote Sensing of Environment*, *202*, 18–27. https://doi.org/10.1016/j.rse.2017.06.031

Greenwell, B. M. (2017). pdp: An R package for constructing partial dependence plots. *The R Journal*, *9*(1), 421–436. https://doi.org/10.32614/RJ-2017-016

Guay, K. C., Beck, P. S. A., Berner, L. T., Goetz, S. J., Baccini, A., & Buermann, W. (2014). Vegetation productivity patterns at high northern latitudes: A multi-sensor satellite data assessment. *Global Change Biology*, *20*(10), 3147–3158. https://doi.org/10.1111/gcb.12647

Guindon, L., Villemaire, P., St-Amant, R., Bernier, P. Y., Beaudoin, A., Caron, F., … Dorion, H. (2017). Canada Landsat Disturbance

(CanLaD): a Canada-wide Landsat-based 30-m resolution product of fire and harvest detection and attribution since 1984. https://doi.org/10.23687/add1346b-f632-4eb9-a83d-a662b38655ad

Hansen, M. C., Potapov, P. V., Moore, R., Hancher, M., Turubanova, S. A., Tyukavina, A., Thau, D., Stehman, S. V., Goetz, S. J., Loveland, T. R., Kommareddy, A., Egorov, A., Chini, L., Justice, C. O., & Townshend, J. R. G. (2013). High-resolution global maps of 21st-century forest cover change. *Science*, *342*(6160), 850. https://doi.org/10.1126/science.1244693

Hellmann, L., Agafonov, L., Ljungqvist, F. C., Churakova (Sidorova), O., Düthorn, E., Esper, J., Hülsmann, L., Kirdyanov, A. V., Moiseev, P., Myglan, V. S., Nikolaev, A. N., Reinig, F., Schweingruber, F. H., Solomina, O., Tegel, W., & Büntgen, U. (2016). Diverse growth trends and climate responses across Eurasia's boreal forest. *Environmental Research Letters*, *11*(7). https://doi.org/10.1088/1748-9326/11/7/074021

Hengl, T., Mendes de Jesus, J., Heuvelink, G. B. M., Ruiperez Gonzalez, M., Kilibarda, M., Blagotić, A., Shangguan, W., Wright, M. N., Geng, X., Bauer-Marschallinger, B., Guevara, M. A., Vargas, R., MacMillan, R. A., Batjes, N. H., Leenaars, J. G. B., Ribeiro, E., Wheeler, I., Mantel, S., & Kempen, B. (2017). SoilGrids250m: Global gridded soil information based on machine learning. *PLoS One*, *12*(2), e0169748. https://doi.org/10.1371/journal.pone.0169748

Hijmans, R. J. (2019). raster: Geographic Analysis and Modeling. R package version 3.0-12. http://CRAN.R-project.org/package=raster

Huemmrich, K. F., Vargas Zesati, S., Campbell, P., & Tweedie, C. (2021). Canopy reflectance models illustrate varying NDVI responses to change in high latitude ecosystems. *Ecological Applications*, *31*(8), e02435. https://doi.org/10.1002/eap.2435

IPCC (2021). *Climate Change 2021: The Physical Science Basis. Contribution of Working Group I to the Sixth Assessment Report of the Intergovernmental Panel on*. Cambridge University Press.

Jiang, Z., Huete, A. R., Didan, K., & Miura, T. (2008). Development of a two-band enhanced vegetation index without a blue band. *Remote Sensing of Environment*, *112*(10), 3833–3845. https://doi.org/10.1016/j.rse.2008.06.006

Johansen, B., & Tømmervik, H. (2014). The relationship between phytomass, NDVI and vegetation communities on Svalbard. *International Journal of Applied Earth Observation and Geoinformation*, *27*, 20–30. https://doi.org/10.1016/j.jag.2013.07.001

Ju, J., & Masek, J. G. (2016). The vegetation greenness trend in Canada and US Alaska from 1984–2012 Landsat data. *Remote Sensing of Environment*, *176*, 1–16. https://doi.org/10.1016/j.rse.2016.01.001

Juday, G. P., & Alix, C. (2012). Consistent negative temperature sensitivity and positive influence of precipitation on growth of floodplain Picea glauca in Interior Alaska. *Canadian Journal of Forest Research*, *42*(3), 561–573. https://doi.org/10.1139/x2012-008

Kasischke, E. S., Williams, D., & Barry, D. (2002). Analysis of the patterns of large fires in the boreal forest region of Alaska. *International Journal of Wildland Fire*, *11*(2), 131–144. https://doi.org/10.1071/WF02023

Kassambara, A. (2020). ggpubr: 'ggplot2' Based Publication Ready Plots. R package version 0.4.0. https://CRAN.R-project.org/package=ggpubr

Keenan, T., & Riley, W. (2018). Greening of the land surface in the world's cold regions consistent with recent warming. *Nature Climate Change*, *8*(9), 825. https://doi.org/10.1038/s41558-018-0258-y

Kharuk, V. I., Im, S. T., Petrov, I. A., Dvinskaya, M. L., Shushpanov, A. S., & Golyukov, A. S. (2020). Climate-driven conifer mortality in Siberia. *Global Ecology and Biogeography*, *30*, 543–556. https://doi.org/10.1111/geb.13243

Kharuk, V. I., Ponomarev, E. I., Ivanova, G. A., Dvinskaya, M. L., Coogan, S. C., & Flannigan, M. D. (2021). Wildfires in the Siberian taiga. *Ambio*, *1–22*, https://doi.org/10.1007/s13280-020-01490-x

Kharuk, V. I., Ranson, K. J., Im, S. T., Oskorbin, P. A., Dvinskaya, M. L., & Ovchinnikov, D. V. (2013). Tree-line structure and dynamics at the northern limit of the larch forest: Anabar Plateau, Siberia, Russia. *Arctic, Antarctic, and Alpine Research*, *45*(4), 526–537. https://doi.org/10.1657/1938-4246-45.4.526

Koven, C. D. (2013). Boreal carbon loss due to poleward shift in low-carbon ecosystems. *Nature Geoscience*, *6*, 452–456. https://doi.org/10.1038/ngeo1801

Kuhn, M. (2008). Building predictive models in R using the caret package. *Journal of Statistical Software*, *28*(5), 1–26.

Kukavskaya, E. A., Buryak, L. V., Shvetsov, E. G., Conard, S. G., & Kalenskaya, O. P. (2016). The impact of increasing fire frequency on forest transformations in southern Siberia. *Forest Ecology and Management*, *382*, 225–235. https://doi.org/10.1016/j.foreco.2016.10.015

Lantz, T. C., Gergel, S. E., & Henry, G. H. (2010). Response of green alder (*Alnus viridis* subsp. *fruticosa*) patch dynamics and plant community composition to fire and regional temperature in north-western Canada. *Journal of Biogeography*, *37*(8), 1597–1610.

Lantz, T. C., Marsh, P., & Kokelj, S. V. (2013). Recent shrub proliferation in the Mackenzie Delta uplands and microclimatic implications. *Ecosystems*, *16*(1), 47–59. https://doi.org/10.1007/s10021-012-9595-2

Lantz, T. C., Moffat, N. D., Fraser, R. H., & Walker, X. (2019). Reproductive limitation mediates the response of white spruce (Picea glauca) to climate warming across the forest–tundra ecotone. *Arctic Science*, *5*(4), 167–184. https://doi.org/10.1139/as-2018-0012

Liaw, A., & Wiener, M. (2002). Classification and Regression by randomForest. *R News*, *2*(3), 18–22.

Lin, X., Rogers, B. M., Sweeney, C., Chevallier, F., Arshinov, M., Dlugokencky, E., & Keppel-Aleks, G. (2020). Siberian and temperate ecosystems shape Northern Hemisphere atmospheric CO2 seasonal amplification. *Proceedings of the National Academy of Sciences*, *117*(35), 21079. https://doi.org/10.1073/pnas.1914135117

Lloyd, A. H., Fastie, C. L., & Eisen, H. (2007). Fire and substrate interact to control the northern range limit of black spruce (Picea mariana) in Alaska. *Canadian Journal of Forest Research*, *37*(12), 2480–2493. https://doi.org/10.1139/x07-092

Loboda, T. V., & Chen, D. (2016). Distribution of young forests and estimated stand age across Russia, 2012. ORNL Distributed Active Archive Center. https://doi.org/10.3334/ORNLDAAC/1330

Loboda, T. V., & Chen, D. (2017). Spatial distribution of young forests and carbon fluxes within recent disturbances in Russia. *Global Change Biology*, *23*(1), 138–153. https://doi.org/10.1111/gcb.13349

Loranty, M., Davydov, S., Kropp, H., Alexander, H., Mack, M., Natali, S., & Zimov, N. (2018). Vegetation indices do not capture forest cover variation in upland Siberian larch forests. *Remote Sensing*, *10*(11), 1686. https://doi.org/10.3390/rs10111686

Maher, C. T., Dial, R. J., Pastick, N. J., Hewitt, R. E., Jorgenson, M. T., & Sullivan, P. F. (2021). The climate envelope of Alaska's northern treelines: Implications for controlling factors and future treeline advance. *Ecography*, *44*(11), 1710–1722. https://doi.org/10.1111/ecog.05597

Mamet, S. D., Brown, C. D., Trant, A. J., & Laroque, C. P. (2019). Shifting global Larix distributions: Northern expansion and southern retraction as species respond to changing climate. *Journal of Biogeography*, *46*(1), 30–44.

Markham, B., Barsi, J., Kvaran, G., Ong, L., Kaita, E., Biggar, S., & Helder, D. (2014). Landsat-8 operational land imager radiometric calibration and stability. *Remote Sensing*, *6*(12), 12275–12308.

Markham, B. L., & Helder, D. L. (2012). Forty-year calibrated record of earth-reflected radiance from Landsat: A review. *Remote Sensing of Environment*, *122*, 30–40. https://doi.org/10.1016/j.rse.2011.06.026

Masek, J. G., Vermote, E. F., Saleous, N. E., Wolfe, R., Hall, F. G., Huemmrich, K. F., Gao, F., Kutler, J., & Lim, T.-K. (2006). A Landsat

surface reflectance dataset for North America, 1990–2000. *IEEE Geoscience and Remote Sensing Letters*, *3*(1), 68–72. https://doi.org/10.1109/LGRS.2005.857030

Michaelian, M., Hogg, E. H., Hall, R. J., & Arsenault, E. (2011). Massive mortality of aspen following severe drought along the southern edge of the Canadian boreal forest. *Global Change Biology*, *17*(6), 2084–2094. https://doi.org/10.1111/j.1365-2486.2010.02357.x

Myers-Smith, I. H., & Hik, D. S. (2018). Climate warming as a driver of tundra shrubline advance. *Journal of Ecology*, *106*(2), 547–560. https://doi.org/10.1111/1365-2745.12817

Myers-Smith, I. H., Kerby, J. T., Phoenix, G. K., Bjerke, J. W., Epstein, H. E., Assmann, J. J., John, C., Andreu-Hayles, L., Angers-Blondin, S., Beck, P. S. A., Berner, L. T., Bhatt, U. S., Bjorkman, A. D., Blok, D., Bryn, A., Christiansen, C. T., Cornelissen, J. H. C., Cunliffe, A. M., Elmendorf, S. C., … Wipf, S. (2020). Complexity revealed in the greening of the Arctic. *Nature Climate Change*, *10*(2), 106–117. https://doi.org/10.1038/s41558-019-0688-1

Myneni, R. B., Keeling, C. D., Tucker, C. J., Asrar, G., & Nemani, R. R. (1997). Increased plant growth in the northern high latitudes from 1981 to 1991. *Nature*, *386*(6626), 698–702.

National Academies of Sciences (2019). *Understanding Northern Latitude Vegetation Greening and Browning: Proceedings of a Workshop*. The National Academies Press.

O'Brien, J. (2019). gdalUtilities: Wrappers for 'GDAL' Utilities Executables. R package version 1. https://CRAN.R-project.org/package=gdalUtilities

Obu, J., Westermann, S., Kääb, A., & Bartsch, A. (2018). Ground temperature map, 2000–2016. *Northern Hemisphere Permafrost*. https://doi.org/10.1594/PANGAEA.888600

Olnes, J., Kielland, K., Juday, G. P., Mann, D. H., Genet, H., & Ruess, R. W. (2017). Can snowshoe hares control treeline expansions? *Ecology*, *98*(10), 2506–2512.

Olson, D. M., Dinerstein, E., Wikramanayake, E. D., Burgess, N. D., Powell, G. V. N., Underwood, E. C., D'amico, J. A., Itoua, I., Strand, H. E., Morrison, J. C., Loucks, C. J., Allnutt, T. F., Ricketts, T. H., Kura, Y., Lamoreux, J. F., Wettengel, W. W., Hedao, P., & Kassem, K. R. (2001). Terrestrial Ecoregions of the World: A New Map of Life on Earth A new global map of terrestrial ecoregions provides an innovative tool for conserving biodiversity. *BioScience*, *51*(11), 933–938.

Pan, Y., Birdsey, R. A., Phillips, O. L., & Jackson, R. B. (2013). The structure, distribution, and biomass of the world's forests. *Annual Review of Ecology, Evolution, and Systematics*, *44*, 593–622. https://doi.org/10.1146/annurev-ecolsys-110512-135914

Parent, M. B., & Verbyla, D. (2010). The browning of Alaska's Boreal Forest. *Remote Sensing*, *2*(12), 2729–2747. https://doi.org/10.3390/rs2122729

Park, T., Ganguly, S., Tømmervik, H., Euskirchen, E. S., Høgda, K.-A., Karlsen, S. R., Brovkin, V., Nemani, R. R., & Myneni, R. B. (2016). Changes in growing season duration and productivity of northern vegetation inferred from long-term remote sensing data. *Environmental Research Letters*, *11*(8). https://doi.org/10.1088/1748-9326/11/8/084001

Pastick, N. J., Jorgenson, M. T., Goetz, S. J., Jones, B. M., Wylie, B. K., Minsley, B. J., Genet, H., Knight, J. F., Swanson, D. K., & Jorgenson, J. C. (2019). Spatiotemporal remote sensing of ecosystem change and causation across Alaska. *Global Change Biology*, *25*(3), 1171–1189. https://doi.org/10.1111/gcb.14279

Paulsen, J., & Körner, C. (2014). A climate-based model to predict potential treeline position around the globe. *Alpine Botany*, *124*(1), 1–12. https://doi.org/10.1007/s00035-014-0124-0

Pekel, J.-F., Cottam, A., Gorelick, N., & Belward, A. S. (2016). High-resolution mapping of global surface water and its long-term changes. *Nature*, *540*(7633), 418–422. https://doi.org/10.1038/nature20584

Peng, C., Ma, Z., Lei, X., Zhu, Q., Chen, H., Wang, W., Liu, S., Li, W., Fang, X., & Zhou, X. (2011). A drought-induced pervasive increase in tree mortality across Canada's boreal forests. *Nature Climate Change*, *1*(9), 467–471. https://doi.org/10.1038/nclimate1293

Peng, X., Zhang, T., Frauenfeld, O. W., Wang, S., Qiao, L., Du, R., & Mu, C. (2020). Northern Hemisphere Greening in Association With Warming Permafrost. *Journal of Geophysical Research: Biogeosciences*, *125*(1), e2019JG005086. https://doi.org/10.1029/2019jg005086

Perkins-Kirkpatrick, S., & Gibson, P. (2017). Changes in regional heatwave characteristics as a function of increasing global temperature. *Scientific Reports*, *7*(1), 1–12. https://doi.org/10.1038/s41598-017-12520-2

Piao, S., Wang, X., Park, T., Chen, C., Lian, X. U., He, Y., Bjerke, J. W., Chen, A., Ciais, P., Tømmervik, H., Nemani, R. R., & Myneni, R. B. (2020). Characteristics, drivers and feedbacks of global greening. *Nature Reviews Earth & Environment*, *1*(1), 14–27. https://doi.org/10.1038/s43017-019-0001-x

R Core Team (2021). *R: A Language and Environment for Statistical Computing*. R Foundation for Statistical Computing.

Raynolds, M. K., Comiso, J. C., Walker, D. A., & Verbyla, D. (2008). Relationship between satellite-derived land surface temperatures, arctic vegetation types, and NDVI. *Remote Sensing of Environment*, *112*(4), 1884–1894. https://doi.org/10.1016/j.rse.2007.09.008

Rees, W. G., Hofgaard, A., Boudreau, S., Cairns, D. M., Harper, K., Mamet, S., Mathisen, I., Swirad, Z., & Tutubalina, O. (2020). Is subarctic forest advance able to keep pace with climate change? *Global Change Biology*, *26*, 3965–3977. https://doi.org/10.1111/gcb.15113

Refsland, T. K., & Cushman, J. H. (2021). Continent-wide synthesis of the long-term population dynamics of quaking aspen in the face of accelerating human impacts. *Oecologia*, *197*, 25–42. https://doi.org/10.1007/s00442-021-05013-7

Rogers, B. M., Solvik, K., Hogg, E. H., Ju, J., Masek, J. G., Michaelian, M., Berner, L. T., & Goetz, S. J. (2018). Detecting early warning signals of tree mortality in boreal North America using multiscale satellite data. *Global Change Biology*, *24*(6), 2284–2304. https://doi.org/10.1111/gcb.14107

Ropars, P., Lévesque, E., & Boudreau, S. (2015). How do climate and topography influence the greening of the forest-tundra ecotone in northern Québec? A dendrochronological analysis of Betula glandulosa. *Journal of Ecology*, *103*(3), 679–690.

Rouse, J., Haas, R., Schell, J., & Deering, D. (1974). Monitoring vegetation systems in the Great Plains with ERTS. *NASA Special Publication*, *351*, 309–317.

Sayre, R., Dangermond, J., Frye, C., Vaughan, R., Aniello, P., Breyer, S., & Derrenbacher, W. (2014). *A new map of global ecological land units—an ecophysiographic stratification approach*. Association of American Geographers.

Scheffer, M., Hirota, M., Holmgren, M., Van Nes, E. H., & Chapin, F. S. (2012). Thresholds for boreal biome transitions. *Proceedings of the National Academy of Sciences*, *109*(52), 21384–21389. https://doi.org/10.1073/pnas.1219844110

Sellers, P. (1987). Canopy reflectance, photosynthesis, and transpiration, II. The role of biophysics in the linearity of their interdependence. *Remote Sensing of Environment*, *21*(2), 143–183.

Sexton, J. O., Noojipady, P., Song, X.-P., Feng, M., Song, D.-X., Kim, D.-H., & Pimm, S. L. (2016). Conservation policy and the measurement of forests. *Nature Climate Change*, *6*(2), 192–196.

Stöcklin, J., & Körner, C. (1999). Recruitment and mortality of Pinus sylvestris near the nordic treeline: The role of climatic change and herbivory. *Ecological Bulletins*, *47*, 168–177.

Stralberg, D., Wang, X., Parisien, M.-A., Robinne, F.-N., Sólymos, P., Mahon, C. L., Nielsen, S. E., & Bayne, E. M. (2018). Wildfire-mediated vegetation change in boreal forests of Alberta. *Canada. Ecosphere*, *9*(3), e02156. https://doi.org/10.1002/ecs2.2156

Sulla-Menashe, D., Woodcock, C., & Friedl, M. A. (2017). Canadian boreal forest greening and browning trends: an analysis of biogeographic patterns and the relative roles of disturbance versus climate drivers. *Environmental Research Letters*, *13*, https://doi.org/10.1088/1748-9326/aa9b88

Sullivan, P. F., Pattison, R. R., Brownlee, A. H., Cahoon, S. M., & Hollingsworth, T. N. (2017). Limited evidence of declining growth among moisture-limited black and white spruce in interior Alaska. *Scientific Reports*, *7*(1), 15344. https://doi.org/10.1038/s41598-017-15644-7

Tchebakova, N. M., Parfenova, E., & Soja, A. J. (2009). The effects of climate, permafrost and fire on vegetation change in Siberia in a changing climate. *Environmental Research Letters*, *4*(4). https://doi.org/10.1088/1748-9326/4/4/045013

Timoney, K. P., Mamet, S. D., Cheng, R., Lee, P., Robinson, A. L., Downing, D., & Wein, R. W. (2019). Tree cover response to climate change in the forest-tundra of north-central Canada: fire-driven decline, not northward advance. *Ecoscience*, *26*(2), 133–148. https://doi.org/10.1080/11956860.2018.1532868

Trant, A. J., & Hermanutz, L. (2014). Advancing towards novel tree lines? A multispecies approach to recent tree line dynamics in subarctic alpine Labrador, northern Canada. *Journal of Biogeography*, *41*(6), 1115–1125. https://doi.org/10.1111/jbi.12287

Van Bogaert, R., Haneca, K., Hoogesteger, J., Jonasson, C., De Dapper, M., & Callaghan, T. V. (2011). A century of tree line changes in sub-Arctic Sweden shows local and regional variability and only a minor influence of 20th century climate warming. *Journal of Biogeography*, *38*(5), 907–921. https://doi.org/10.1111/j.1365-2699.2010.02453.x

Venter, O., Sanderson, E. W., Magrach, A., Allan, J. R., Beher, J., Jones, K. R., Possingham, H. P., Laurance, W. F., Wood, P., Fekete, B. M., Levy, M. A., & Watson, J. E. M. (2016). Global terrestrial Human Footprint maps for 1993 and 2009. *Scientific Data*, *3*, 160067. https://doi.org/10.1038/sdata.2016.67

Verdonen, M., Berner, L. T., Forbes, B. C., & Kumpula, T. (2020). Periglacial vegetation dynamics in Arctic Russia: decadal analysis of tundra regeneration on landslides with time series satellite imagery. *Environmental Research Letters*, *15*, 105020. https://doi.org/10.1088/1748-9326/abb500

Vermote, E., Justice, C., Claverie, M., & Franch, B. (2016). Preliminary analysis of the performance of the Landsat 8/OLI land surface reflectance product. *Remote Sensing of Environment*, *185*, 46–56. https://doi.org/10.1016/j.rse.2016.04.008

Walker, D., Epstein, H., Jia, G., Balser, A., Copass, C., Edwards, E., & Maier, H. (2003). Phytomass, LAI, and NDVI in northern Alaska: relationships to summer warmth, soil pH, plant functional types, and extrapolation to the circumpolar Arctic. *Journal of Geophysical Research*, *108*(D2), 8169. https://doi.org/10.1029/2001JD000986

Walker, X. J., Alexander, H. D., Berner, L. T., Boyd, M. A., Loranty, M. M., Natali, S. M., & Mack, M. C. (2021). Positive response of tree productivity to warming is reversed by increased tree density at the Arctic tundra-taiga ecotone. *Canadian Journal of Forest Research*, *51*(9), 1323–1338. https://doi.org/10.1139/cjfr-2020-0466

Walker, X. J., Rogers, B. M., Veraverbeke, S., Johnstone, J. F., Baltzer, J. L., Barrett, K., Bourgeau-Chavez, L., Day, N. J., de Groot, W. J., Dieleman, C. M., Goetz, S., Hoy, E., Jenkins, L. K., Kane, E. S., Parisien, M.-A., Potter, S., Schuur, E. A. G., Turetsky, M., Whitman, E., & Mack, M. C. (2020). Fuel availability not fire weather controls boreal wildfire severity and carbon emissions. *Nature Climate Change*, *10*(12), 1130–1136. https://doi.org/10.1038/s41558-020-00920-8

Wang, J. A., Baccini, A., Farina, M., Randerson, J. T., & Friedl, M. A. (2021). Disturbance suppresses the aboveground carbon sink in North American boreal forests. *Nature Climate Change*, *11*, 435–441. https://doi.org/10.1038/s41558-021-01027-4

Wang, J. A., & Friedl, M. A. (2019). The role of land cover change in Arctic-Boreal greening and browning trends. *Environmental Research Letters*, *14*(12), 125007. https://doi.org/10.1088/1748-9326/ab5429

Wang, J. A., Sulla-Menashe, D., Woodcock, C. E., Sonnentag, O., Keeling, R. F., & Friedl, M. A. (2019). Extensive land cover change across Arctic-Boreal Northwestern North America from disturbance and climate forcing. *Global Change Biology*, *26*, 807–822. https://doi.org/10.1111/gcb.14804

Welp, L. R., Patra, P. K., Rödenbeck, C., Nemani, R., Bi, J., Piper, S. C., & Keeling, R. F. (2016). Increasing summer net CO2 uptake in high northern ecosystems inferred from atmospheric inversions and comparisons to remote-sensing NDVI. *Atmospheric Chemistry and Physics*, *16*(14), 9047–9066. https://doi.org/10.5194/acp-16-9047-2016

Whitman, E., Parisien, M.-A., Thompson, D. K., & Flannigan, M. D. (2019). Short-interval wildfire and drought overwhelm boreal forest resilience. *Scientific Reports*, *9*(1), 18796. https://doi.org/10.1038/s41598-019-55036-7

Wickham, H. (2016). *ggplot2: Elegant graphics for data analysis*. Springer-Verlang New York.

Wickham, H. (2021). tidyr: Tidy Messy Data. R package version 1.1.4. https://CRAN.R-project.org/package=tidyr

Wickham, H., Francois, R., Lionel, H., & Müller, K. (2021). dplyr: A Grammar of Data Manipulation. R package version 1.0.7. https://CRAN.R-project.org/package=dplyr

Wieczorek, M., Kruse, S., Epp, L. S., Kolmogorov, A., Nikolaev, A. N., Heinrich, I., & Herzschuh, U. (2017). Dissimilar responses of larch stands in northern Siberia to increasing temperatures—a field and simulation based study. *Ecology*, *98*(9), 2343–2355.

Wulder, M. A., Loveland, T. R., Roy, D. P., Crawford, C. J., Masek, J. G., Woodcock, C. E., Allen, R. G., Anderson, M. C., Belward, A. S., Cohen, W. B., Dwyer, J., Erb, A., Gao, F., Griffiths, P., Helder, D., Hermosilla, T., Hipple, J. D., Hostert, P., Hughes, M. J., … Zhu, Z. (2019). Current status of Landsat program, science, and applications. *Remote Sensing of Environment*, *225*, 127–147. https://doi.org/10.1016/j.rse.2019.02.015

Wulder, M. A., White, J. C., Loveland, T. R., Woodcock, C. E., Belward, A. S., Cohen, W. B., Fosnight, E. A., Shaw, J., Masek, J. G., & Roy, D. P. (2016). The global Landsat archive: Status, consolidation, and direction. *Remote Sensing of Environment*, *185*, 271–283. https://doi.org/10.1016/j.rse.2015.11.032

Yue, S., Pilon, P., Phinney, B., & Cavadias, G. (2002). The influence of autocorrelation on the ability to detect trend in hydrological series. *Hydrological Processes*, *16*(9), 1807–1829. https://doi.org/10.1002/hyp.1095

Zhu, Z., Wang, S., & Woodcock, C. E. (2015). Improvement and expansion of the Fmask algorithm: cloud, cloud shadow, and snow detection for Landsats 4–7, 8, and Sentinel 2 images. *Remote Sensing of Environment*, *159*, 269–277. https://doi.org/10.1016/j.rse.2014.12.014

SUPPORTING INFORMATION

Additional supporting information may be found in the online version of the article at the publisher's website.

How to cite this article: Berner, L. T., & Goetz, S. J. (2022). Satellite observations document trends consistent with a boreal forest biome shift. *Global Change Biology*, 28, 3275–3292. https://doi.org/10.1111/gcb.16121